

**NISTIR 5321**

---

---

**A Study of Heat Pump Performance Using  
Mixtures of R32/R134a and R32/R125/R134a as  
"Drop-In" Working Fluids for R22 With  
and Without a Liquid-Suction Heat Exchanger**

---

---

Peter I. Rothfleisch  
David A. Didion

Building and Fire Research Laboratory  
Gaithersburg, Maryland 20899

**NIST**

**United States Department of Commerce  
Technology Administration  
National Institute of Standards and Technology**

QC

100

.U56

# 5321

1993



## A Study of Heat Pump Performance Using Mixtures of R32/R134a and R32/R125/R134a as "Drop-In" Working Fluids for R22 With and Without a Liquid-Suction Heat Exchanger

---

---

Peter I. Rothfleisch  
David A. Didion

December 1993



U.S. Department of Commerce  
Ronald H. Brown, *Secretary*  
Technology of Administration  
Mary L. Good, *Under Secretary for Technology*  
National Institute of Standards and Technology  
Arati Prabhakar, *Director*

*Prepared for:*  
U.S. Department of Energy  
John Ryan, *Director*  
Esher Kweller, *Project Manager*  
Building Equipment Division  
Conservation and Renewable Energy  
1000 Independence Ave., Sw  
Washington, DC 20585

*Prepared for:*  
U.S. Environmental Protection Agency  
Robert V. Hendriks, *Project Officer*  
Air & Energy Engineering Research Lab  
Research Triangle Park, NC 27711



## ABSTRACT

A ductless mini-split residential heat pump with a modified indoor coil was utilized to compare the performance of R22 and a mixture of 34% R32/66% R134a by weight. This test was intended to serve as an indicator of "drop-in" performance so the system was optimized for each refrigerant by varying only the charge mass and expansion valve setting. At the 27.8°C (82°F) cooling test condition the capacity and COP of the mixture were 94% and 90% of the values for R22, respectively. Additional tests were conducted with a liquid-suction intracycle heat exchanger. The modified system was operated with both single-phase and two-phase refrigerant entering the low pressure side of the liquid-suction heat exchanger. The addition of the liquid-suction heat exchanger showed a minimal performance improvement with the performance of the two-phase variation being slightly higher. The best performing liquid-suction heat exchanger variant (two-phase refrigerant on the low pressure side) was also run with a ternary mixture of 30% R32/10% R125/60% R134a, by weight. The results for this mixture were similar to the binary mixture. To examine how well the drop-in test results reflect the fluids performance potential an ideal cycle computer model was used in conjunction with test data to calculate the total UA per unit capacity for each fluid. These results showed that the combination of this system and test procedure penalized the mixture performance by causing it to have a total UA per unit capacity 18.9% lower than R22. Therefore, these drop-in results are not a true indication of the performance potential of this mixture. The ideal cycle model was also used to show that a pure counterflow air-to-refrigerant evaporator would be beneficial to the performance of a cooling only unit regardless of the heat exchange configuration of the condenser.

## ACKNOWLEDGEMENTS

This study was conducted under the sponsorship of the U.S. Department of Energy, Conservation Branch with Mr. Terry Statt and Mr. Esher Kweller, program managers of Advanced Refrigeration Systems. Funds were also contributed by the U.S. Environmental Protection Agency, Research Triangle Park, N.C. under the management of Mr. Robert Hendriks.

TABLE OF CONTENTS

TABLE OF CONTENTS . . . . .	v
LIST OF FIGURES . . . . .	vi
LIST OF TABLES . . . . .	viii
INTRODUCTION . . . . .	1
BACKGROUND . . . . .	4
A. Interpreting Pressure - Temperature Phase Diagrams . . . . .	4
B. Single phase liquid-suction intracycle heat exchange basics . . . . .	10
C. Two phase liquid-suction heat exchange . . . . .	12
DROP-IN TEST PROCEDURE . . . . .	15
DROP-IN TEST RESULTS . . . . .	23
ANALYSIS OF DROP-IN TEST RESULTS . . . . .	27
LEGITIMACY OF THE DROP-IN TEST AS A BASIS FOR COMPARING THE TWO REFRIGERANTS . . . . .	33
LIQUID-SUCTION HEAT EXCHANGER TESTS . . . . .	36
ANALYSIS OF SINGLE PHASE LIQUID-SUCTION HEAT EXCHANGE RESULTS . . . . .	37
ANALYSIS OF TWO PHASE LIQUID-SUCTION HEAT EXCHANGE RESULTS . . . . .	39
TERNARY REFRIGERANT MIXTURE TEST . . . . .	40
GENERAL CONCLUSIONS REGARDING THE USE OF MIXTURES IN AIR-TO-AIR RESIDENTIAL HEAT PUMPS . . . . .	41
REFERENCES . . . . .	47
APPENDIX A . . . . .	49
APPENDIX B . . . . .	53

## LIST OF FIGURES

1. VAPOR PRESSURE ON $\ln(P)$ vs. $-1/T$ COORDINATES FOR THE PURE COMPONENTS. . . . .	5
2. VAPOR PRESSURE ON $\ln(P)$ vs. $-1/T$ COORDINATES FOR R22 AND THE BINARY MIXTURE OF 34% R32/66% R134a BY WEIGHT . . . . .	5
3. VAPOR PRESSURE ON $\ln(P)$ vs. $-1/T$ COORDINATES FOR R22 AND THE TERNARY MIXTURE OF 30% R32/10% R125/ 60% R134a BY WEIGHT . . . . .	6
4. HARDWARE SCHEMATICS FOR BASIC AND LIQUID-SUCTION HEAT EXCHANGER CYCLES. . . . .	10
5. P-H DIAGRAM FOR BASIC AND LIQUID-SUCTION HEAT EXCHANGE CYCLES . . . . .	11
6. P-H DIAGRAM FOR TWO-PHASE LIQUID-SUCTION HEAT EXCHANGE CYCLE . . . . .	12
7. T-S DIAGRAM FOR PURE FLUID TWO-PHASE LIQUID- SUCTION HEAT EXCHANGE. . . . .	13
8. T-S DIAGRAM FOR ZEOTROPIC MIXTURE TWO-PHASE LIQUID-SUCTION HEAT EXCHANGE . . . . .	13
9. R22 COOLING MODE CHARGE OPTIMIZATION AT THE 35°C (95°F) RATING POINT . . . . .	16
10. 34% R32/66% R134a COOLING MODE CHARGE OPTIMIZATION AT THE 35°C (95°F) RATING POINT . . . . .	16
11. R22 HEATING MODE OPTIMIZATION OF CHARGE AND EXPANSION VALVE SETTING AT THE 35°C (95°F) RATING POINT . . . . .	17
12. VARIATION OF CAPACITY WITH SUBCOOLING. . . . .	19
13. VARIATION OF POWER WITH SUBCOOLING . . . . .	19
14. VARIATION OF CONDENSER PRESSURE WITH SUBCOOLING . . . . .	20
15. CAPACITY AT THE RATING POINTS FOR R22 AND THE MIXTURE . . . . .	26
16. P-H DIAGRAM FOR R22 AND 34% R32/66% R134a . . . . .	30
17. T-S DIAGRAM FOR R22 AND 34% R32/66% R134a . . . . .	30

18. COOLING MODE BOTTOM CIRCUIT EVAPORATOR TEMPERATURE PROFILES . . . . .	31
19. COOLING MODE TOP CIRCUIT EVAPORATOR TEMPERATURE PROFILES . . . . .	31
20. BOTTOM CIRCUIT WITH AND WITHOUT TWO-PHASE LIQUID-SUCTION HEAT EXCHANGE . . . . .	39
21. TOP CIRCUIT WITH AND WITHOUT TWO-PHASE LIQUID-SUCTION HEAT EXCHANGE . . . . .	39
22. LINEARIZATION OF BINARY MIXTURE GLIDE BY THE ADDITION OF A THIRD COMPONENT. . . . .	42
23. VARIATION OF COP WITH UA DISTRIBUTION FOR THE INFINITE HEAT CAPACITY CONDENSER HTF MODEL . . . .	43
24. COP DIFFERENCE OF THE TWO GLIDE MATCH LIMITS FOR THE INFINITE HEAT CAPACITY CONDENSER HTF MODEL . . . .	43
25. R22 COMPONENT ENTROPY GENERATION FOR THE INFINITE HEAT CAPACITY CONDENSER HTF MODEL . . . .	44
26. LINEAR TERNARY COMPONENT ENTROPY GENERATION FOR THE INFINITE HEAT CAPACITY CONDENSER HTF MODEL . . .	44
27. VARIATION OF COP WITH UA DISTRIBUTION FOR THE CROSSFLOW CONDENSER MODEL . . . . .	45
28. DIFFERENCE IN COP BETWEEN EACH MIXTURE AND R22 FOR THE CROSSFLOW CONDENSER MODEL . . . . .	45

## LIST OF TABLES

1. COOLING MODE TEST RESULTS . . . . .	24
2. HEATING MODE TEST RESULTS . . . . .	25
3. NORMALIZED PERFORMANCE VALUES . . . . .	26
4. REFRIGERANT CAPACITY POTENTIAL: 35 °C (95 °F) COOLING MODE PERFORMANCE COMPARISON . . . . .	29
5. VERIFICATION OF CYCLE11 AS A TOOL FOR PREDICTING RELATIVE PERFORMANCE TRENDS . . . . .	34
6. CYCLE11 RELATIVE UA CALCULATIONS . . . . .	34
7. NORMALIZED PERFORMANCE WITH THE LIQUID-SUCTION HEAT EXCHANGER . . . . .	36
8. EFFECT OF TWO-PHASE LIQUID-SUCTION HEAT EXCHANGER . . . . .	40
9. NORMALIZED TERNARY PERFORMANCE . . . . .	40

## INTRODUCTION

The recently invoked regulations restricting the availability of chloroflourocarbons (CFC's) and hydrochloroflourocarbons (HCFC's) have generated considerable interest in replacement refrigerants. The latest revision of the Montreal Protocol requires that a potential alternative refrigerant not be ozone depleting. In addition, practical considerations require that a new refrigerant also be nontoxic, nonflammable, chemically stable and compatible with economically feasible equipment materials. An environmentally acceptable replacement refrigerant should also be at least as thermodynamically efficient as its predecessor in order not to increase global warming.

Even if a substitute refrigerant met all of the above criteria, differences in thermodynamic and transport properties would probably necessitate some new equipment redesign. For example, a loss in refrigerant volumetric capacity could be compensated for by increasing compressor displacement. Changes in pressure drops and heat transfer coefficients may require reevaluation of pipe and heat exchanger sizes, respectively. Equipment manufacturers can respond to these problems by redesigning a product line to optimize the machinery for the new refrigerant. Manufacturers may also choose to make changes in the basic thermodynamic cycle. For example, the addition of a liquid-suction intracycle heat exchanger has been shown to be theoretically capable of increasing the performance of some refrigerants [1].

For the owners of existing equipment, redesigning the system is often not a viable option. In large tonnage applications, such as office buildings and process industries, the existing equipment usually represents a significant monetary investment. Additionally, the building structure is often to some extent designed and built around the refrigeration or HVAC system. These two circumstances can make system replacement impractical and prohibitively expensive. For residential applications, where equipment costs are much lower, the labor costs of replacing major system components could make replacing the entire system an economically competitive alternative. In light of the considerable expenditures faced by equipment owners, a new refrigerant that requires only minor equipment changes would be an ideal substitute. Such alternative refrigerants are commonly referred to as "drop-in" refrigerants.

The primary purpose of this study was to experimentally evaluate how a zeotropic refrigerant mixture of 34% R32 and 66% R134a by weight would perform as a drop-in replacement for R22 in a split-system residential air-source heat pump. The system was of a type that would normally be encountered in the field except for the custom built indoor coil. The indoor coil was constructed with

a large amount of instrumentation and a cross-counter flow configuration (referenced to cooling mode). The binary mixture composition was selected for three reasons. First, both of its components are not ozone depleting. Second, the mixture has a saturated pressure-temperature relationship similar to R22. This requirement must be satisfied so that the pressure limitations of the equipment are not exceeded. Third, previous work at NIST utilizing a water-to-water heat pump with counterflow heat exchange has shown this composition to be capable of giving a volumetric capacity and coefficient of performance (COP) equal to that of R22 [2].

To keep these tests representative of a true drop-in refrigerant change, it was necessary to define what system modifications would be allowed for each refrigerant. For the purposes of this study, the only modifications that were allowed were the adjustment of a hand operated expansion valve and the variation of the refrigerant charge mass. In cooling mode, the system was optimized for each refrigerant (to the extent allowed by the previously defined drop-in restrictions) by varying the expansion valve setting and refrigerant charge to produce a point of maximum COP at the 35°C (95°F) rating point. To simulate the operation of a fixed area expansion device, the 27.8°C (82°F) test was run without any further system modifications. In heating mode, the optimization procedure was repeated at the 8.3°C (47°F) rating point. However, since the designed optimization procedure proved to be governed by the condenser, and since the condenser was of a different heat exchange configuration in the two modes (crossflow in cooling and cross-parallel flow in heating), there was no practically attainable maximum COP point in heating mode. Therefore, an operating point was selected based on practical system considerations. The details of the optimization procedure for both modes are explained in a subsequent section of this report.

At the 35°C (95°F) rating point, where performance was optimized for each fluid, the capacity and COP of the binary mixture were seven and eleven percent below that of R22, respectively. Because of these poor results, and because the mixture is composed primarily of R134a which is a fluid that should theoretically benefit from liquid-suction heat exchange, an additional series of tests were run with a liquid-suction heat exchanger. The liquid-suction heat exchanger was a typical off-the-shelf type of a practical size. Tests with the liquid-suction heat exchanger were performed in the cooling mode only.

Finally, an additional series of tests were conducted with a ternary mixture consisting of 30% R32, 10% R125 and 60% R134a by weight. The ternary is one of the fluids on the ARI R22 substitute finalist list. Because of the performance improvements shown by the addition of the liquid-suction heat exchanger, the ternary was tested only in cooling mode with a liquid-suction heat exchanger.

The heat pump used in this experiment was a ductless mini-split made by a Japanese manufacturer. Several modifications were made to make the system more suitable to experimental work. The compressor was replaced with a commercially available model of approximately the same capacity. The primary reason for replacing the compressor was to make the system compatible with the voltage and frequency which were available in the laboratory. Other modifications consisted of adding a suction accumulator and replacing the system's expansion device with a hand operated expansion valve. Additionally, the indoor coil was replaced by a specially designed heat exchanger which acted in a cross-counter flow pattern for the cooling mode and a cross-parallel flow pattern for the heating mode. The instrumentation and test conditions were as specified in ASHRAE Standard 116-1983. The instrumentation and test apparatus were the same as ref. [3] except for the addition of a chilled mirror dewpoint system for the measurement of humidity.

## BACKGROUND

### A. Interpreting Pressure - Temperature Phase Diagrams

One of the most important considerations for a substitute refrigerant is that the saturated vapor pressure should be similar to the fluid that it is replacing. If this criterion is not met, new systems will require extensive redesigns. For example, a potential R22 substitute is the mixture of 60% R32 and 40% R125. The high vapor pressure and high suction vapor density of this fluid give it a much greater volumetric capacity than R22. If this fluid were to be used as a drop-in substitute, the additional compression work could overload the system's electric motor. Additionally, the increased refrigerant mass flow would cause excessive pressure drops. Difficulties may also be encountered if the fluid pressure exceeds the pressure rating of any system pressure vessels (i.e., compressor shell and suction accumulator). Problems would also occur if a refrigerant with a much lower vapor pressure were dropped-in to a system. For example, consider using pure R134a as a drop-in replacement for R22. The lower suction pressure and density of R134a would cause a drop in capacity that would be unacceptable in almost any application. Therefore, it is not feasible to drop-in a substitute fluid with a vapor pressure much different than that of the fluid for which the system was designed.

A simple way to ascertain the suitability of a substitute refrigerant or refrigerant mixture is to examine the saturated pressure temperature relationship on  $\ln(P)$  vs.  $(-1/T)$  coordinates. This type of graph is shown for the pure refrigerants R22, R134a, R125 and R32 in Figure 1. The Figure shows that all of these fluids have vapor pressures that are considerably different than R22. Therefore, none of these pure fluids would make an acceptable substitute for R22 without extensive system modifications. However, mixtures of these fluids may match the vapor pressure of R22.

For the sake of simplicity let us first consider a binary mixture. For the vapor pressure of a binary zeotropic mixture to match that of R22, the vapor pressure of R22 must be between the vapor pressure of the mixture's pure components. From Figure 1 it is evident that mixtures of R134a with either R125 or R32 could be capable of producing a vapor pressure similar to that of R22. In Figure 2, The vapor pressure is shown on  $\ln(P)$  vs.  $(-1/T)$  coordinates for R22 and the saturated liquid (bubble) and vapor (dew) lines for the binary mixture of 34% R32 and 66% R134a by weight. The mixture vapor pressure (the pressure that would be measured in a vessel containing both liquid and vapor in thermal equilibrium) is a quality dependent value that lies between the dew and bubble line pressures. Figure 2 shows that the mixture has a

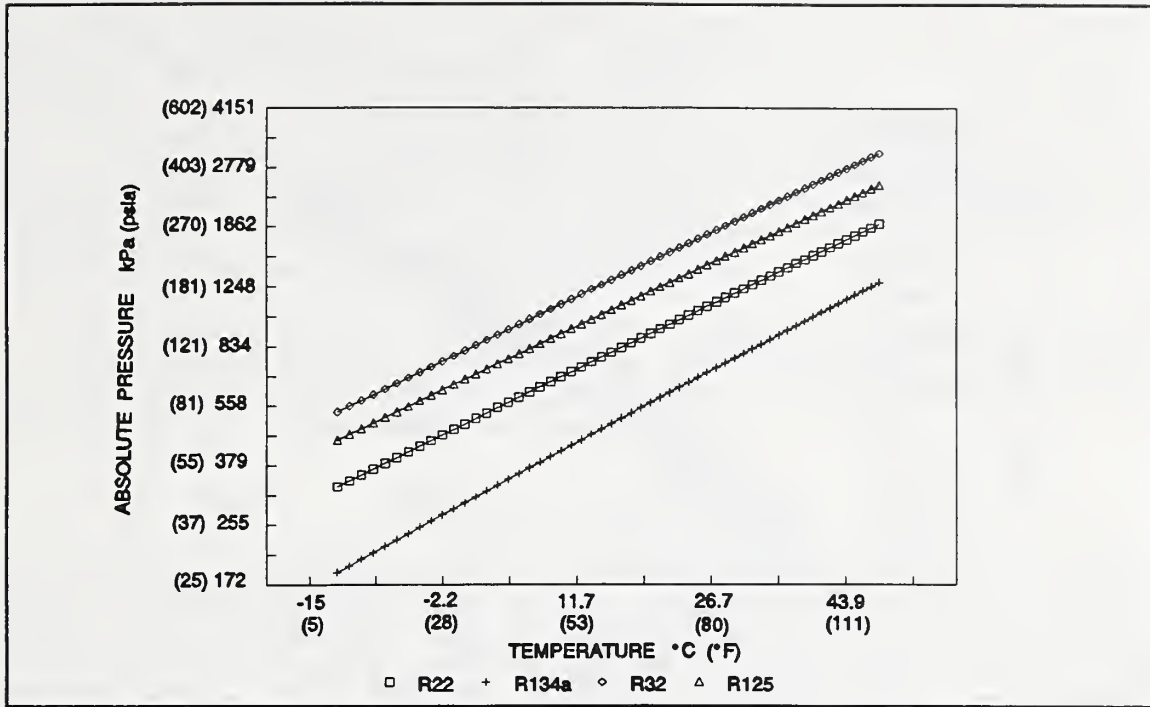


Figure 1 Vapor Pressure on  $\ln(P)$  vs.  $-1/T$  Coordinates for the Pure Components

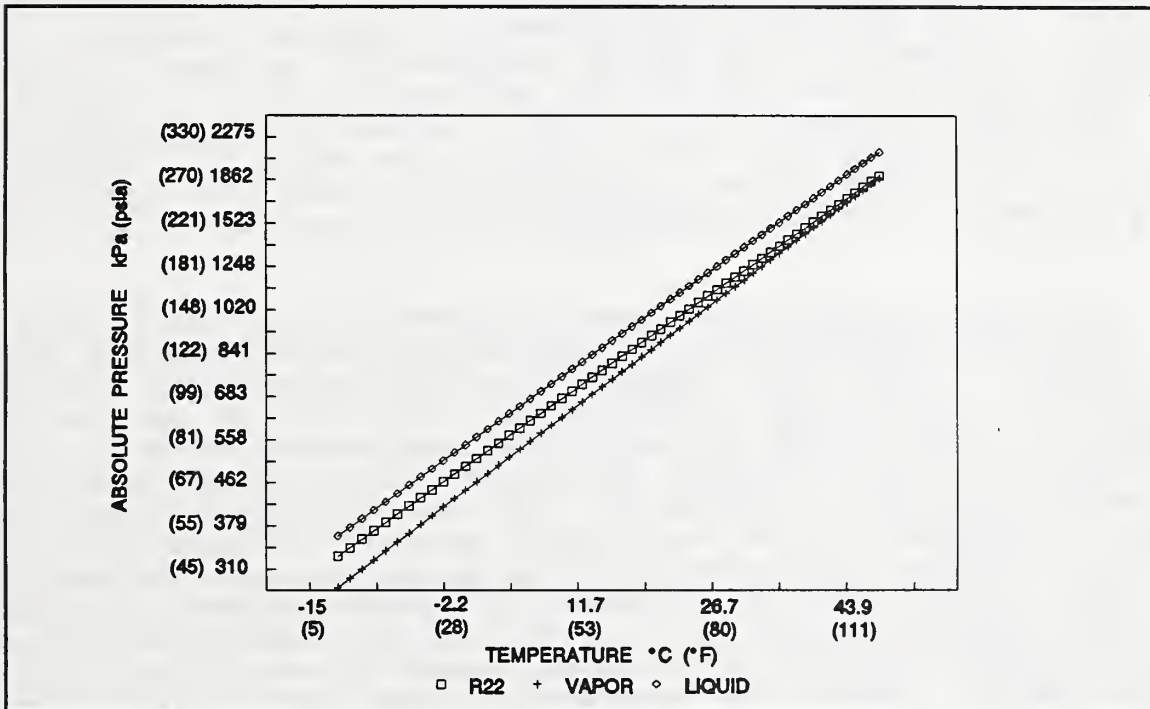
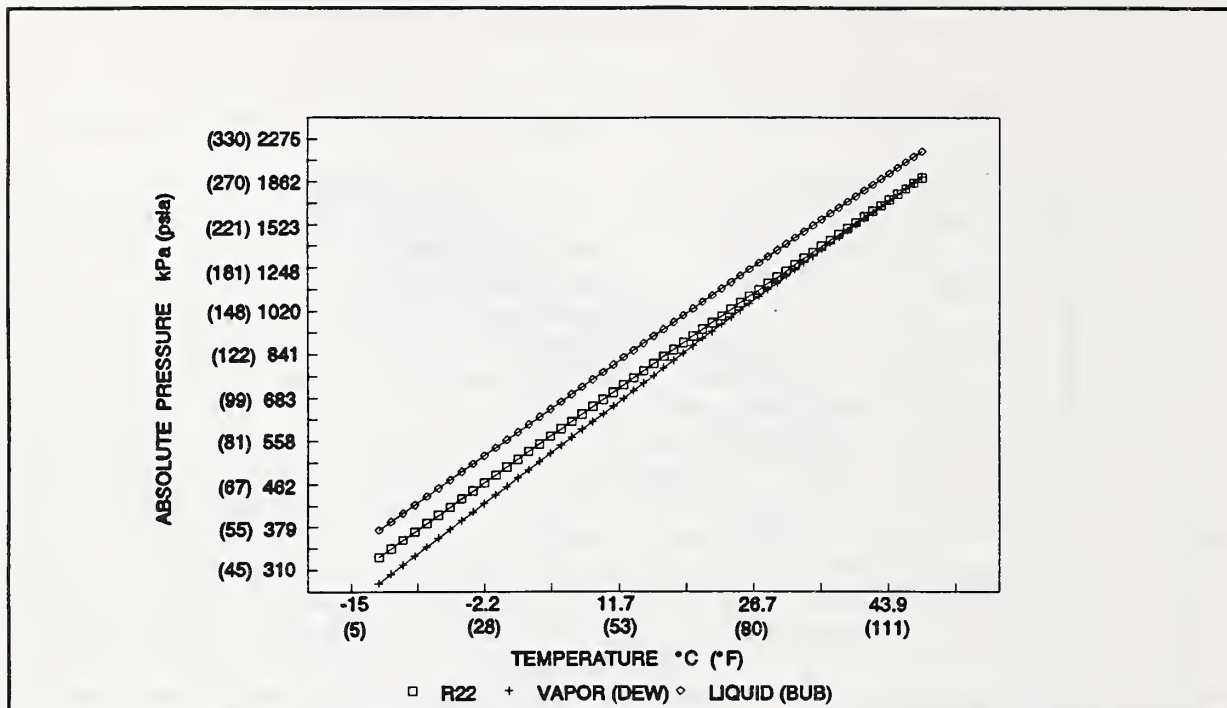


Figure 2 Vapor Pressure on  $\ln(P)$  vs.  $-1/T$  Coordinates for R22 and the Binary Mixture of 34% R32/66% R134a by Weight



**Figure 3** Vapor Pressure on  $\ln(P)$  vs.  $-1/T$  Coordinates for R22 and the Ternary Mixture of 30% R32/10% R125/60% R134a by weight

vapor pressure nearly identical to R22 in the temperature range encountered in heat pump evaporators, but it will have a vapor pressure higher than R22 in the condensing temperature range. This property difference will cause the mixture to have a higher compression ratio than R22 for the same application. In Figure 3, the same graph is shown for a ternary mixture of 30% R32, 10% R125 and 60% R134a by weight. This mixture also exhibits a saturated vapor pressure that is not parallel to the vapor pressure of R22 over the range of temperatures encountered in residential heat pump applications.

A  $\ln(P)$  vs.  $(-1/T)$  graph such as Figure 1, can also be used to estimate the volumetric capacity and COP of a given working fluid relative to another. In general, the high vapor pressure fluids (which lie to the left in Figure 1) will tend to have a high volumetric capacity and low COP. Whereas the low vapor pressure fluids (which lie to the right in Figure 1) will usually have a low volumetric capacity and high COP. The tendency of the high vapor pressure refrigerants to have higher capacities results from the direct relationship between suction pressure and suction density. The high suction density of these refrigerants will give them a high volumetric capacity. The low COP of the high vapor pressure fluids occurs because these fluids tend to have low critical temperatures. Since the saturated liquid line of all fluids flattens out as the critical pressure is approached, the expansion process tends to produce more flash gas as the cycle is operated

closer to the critical point. Additionally, the width of the two-phase dome decreases as the critical point is approached. Therefore, when a cycle operates near the working fluid's critical point the shape of the two-phase dome will cause a reduction in COP. It should be emphasized that the conclusions drawn from Figure 1 are only general tendencies and are also dependent on the pressure level considered. For example, since fluids can have significantly different heat capacities the slopes of vapor pressure curves can cross-over each other.

Additional information regarding the thermodynamic performance of a refrigerant can be gained from examining the basis for the  $\ln(P)$  vs.  $(-1/T)$  coordinates. A well known relation from classical thermodynamics is the Clapeyron equation

$$\left(\frac{dp}{dT}\right)_{\text{sat}} = \frac{h_{fg}}{T(V_g - V_f)} \quad (1)$$

Where  $h_{fg}$  is the latent heat of vaporization,  $v_f$  is the saturated liquid specific volume and  $v_g$  is the saturated vapor specific volume. This equation can be simplified by assuming that the liquid specific volume is negligible in comparison to the vapor specific volume ( $v_g \approx v_g - v_f$ ).

$$\left(\frac{dp}{dT}\right)_{\text{sat}} = \frac{h_{fg}}{TV_g} \quad (2)$$

Next substitute the ideal gas law for  $v_g$  ( $v_g = RT/P$ ), assume that  $h_{fg}$  is constant then separate variables and integrate.

$$\int \frac{dp}{P} = \frac{h_{fg}}{R} \int \frac{dT}{T^2} \quad (3)$$

The final result is

$$\ln P = \frac{h_{fg}}{R} \left(\frac{-1}{T}\right) + C \quad (4)$$

This equation is known as the Clausius-Clapeyron equation. It is an approximate representation of the fluids saturated vapor pressure. The equation is applicable as long as the assumptions implicit in its derivation remain valid. Specifically, the ideal gas law must be approximately valid for the saturated vapor and the latent heat of vaporization must be relatively constant over the temperature range of interest. The most striking feature of the Clausius-Clapeyron equation is that it is in the general linear form  $y=mx+b$ . Figures 1-3, which are derived from accepted property subroutines developed at NIST, are very close to linear in terms of the  $\ln(P)$  vs  $(-1/T)$  coordinates thus, the approximations used to derive the Clausius-Clapeyron equation are felt to be valid for the limited temperature range encountered in residential heat pump applications.

From our knowledge of the general linear form  $y=mx+b$ , we know that the quantity  $m$  represents the slope of the line. In the Clausius-Clapeyron relation, the slope of the line is represented by  $h_{fg}/R$ . This can be converted to another form by eliminating the specific gas constant ( $R$ ) in terms of the universal gas constant ( $R_u$ ). The two gas constants are related by the molecular weight ( $MW$ ) of the substance.

$$R = \frac{R_u}{MW} \quad (5)$$

with this substitution the Clausius-Clapeyron equation becomes

$$\ln P = \frac{h_{fg} (MW)}{R_u} \left( \frac{-1}{T} \right) + C \quad (6)$$

This result shows that with a  $\ln(P)$  vs.  $(-1/T)$  graph, and knowledge of the fluid's molecular weight, the magnitude of the latent heat of one fluid relative to another can be estimated. Alternatively, it may be stated that the molar latent heat determines the slope. Converting equation 3 to a definite integral between the limits of the suction and discharge states and utilizing the universal ideal gas coefficient of equation 5:

$$\int_{P_s}^{P_d} \frac{dp}{P} = \frac{h_{fg} (MW)}{R_u} \int_{T_s}^{T_d} \frac{dT}{T^2} \quad (7)$$

integration yields

$$\ln \left( \frac{P_d}{P_s} \right) = \frac{h_{fg} (MW)}{R_u} \left[ \frac{1}{T_s} - \frac{1}{T_d} \right] \quad (8)$$

multiply both sides by  $(\gamma-1/\gamma)$  and take the exponential

$$\left( \frac{P_d}{P_s} \right)^{\frac{\gamma-1}{\gamma}} = \exp \left[ \left( \frac{\gamma-1}{\gamma} \right) \frac{h_{fg} (MW)}{R_u} \left[ \frac{1}{T_s} - \frac{1}{T_d} \right] \right] \quad (9)$$

which explicitly shows that compression ratio is a function of the latent heat ( $h_{fg}$ ) and molecular weight ( $MW$ ) of the refrigerant. In turn, the compressor work which is equal to the work of compression plus the discharge flow work minus the inlet flow work

$$W = \int P dv + P_d v_d - P_s v_s \quad (10)$$

may be manipulated, via the polytropic relationships among  $P$ - $v$ - $T$ , to yield:

$$W = \frac{\gamma}{\gamma-1} P_s v_s \left\{ \left[ \left( \frac{P_d}{P_s} \right)^{\frac{\gamma-1}{\gamma}} - 1 \right] \right\} \quad (11)$$

substituting in from equation (9):

$$W = \frac{\gamma}{\gamma - 1} P_s V_s \left\{ \exp \left[ \left( \frac{\gamma - 1}{\gamma} \right) \frac{h_{fg} (MW)}{R_u} \left( \frac{1}{T_s} - \frac{1}{T_d} \right) \right] - 1 \right\} \quad (12)$$

which establishes compressor work with the molar latent heat ( $h_{fg}$  MW). Also, since the term  $\left[ \frac{h_{fg} (MW)}{R_u} \right]$  is the slope of the phase line on the  $\ln(P)$  vs  $(-1/T)$  diagram a refrigerant with a steeper slope is one that will require more specific compressor work.

## B. Single phase liquid-suction intracycle heat exchange basics

Among the many possible variations on the basic refrigeration (vapor compression) cycle, the addition of a liquid-suction intracycle heat exchanger is probably the simplest and easiest to implement. This cycle modification consists of subcooling the high pressure liquid refrigerant leaving the condenser with the low pressure vapor leaving the evaporator. Hardware schematics for the basic cycle and the cycle with liquid-suction heat exchange are shown in Figure 4.

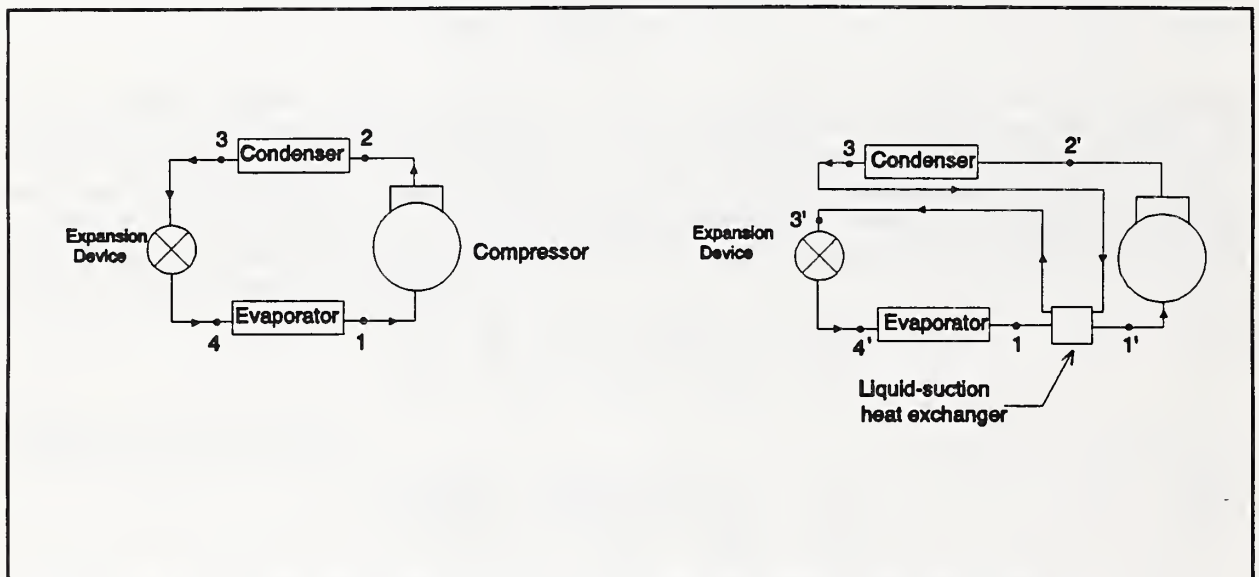


**Figure 4** Hardware Schematics for Basic and Liquid-Suction Heat Exchange Cycles

The effect of the liquid-suction heat exchanger can be easily understood by examining both the basic cycle and the modified cycle on pressure-enthalpy coordinates as shown in Figure 5. Refrigerant state points on the figure that are primed refer to the modified cycle. The figure shows that the heat exchanger produces two competing effects. The positive effect, which tends to increase the system capacity, is caused by the subcooling of the liquid refrigerant from state point 3 to 3'. This causes a reduction in the refrigerant quality entering the evaporator, and a commensurate rise in the latent heat available to produce a useful refrigerating effect. The same amount of heat removed in the subcooling process is picked up by the vapor leaving the evaporator. This causes the vapor to be superheated from state point 1 to 1'. The additional superheat picked up by the vapor has a detrimental effect on system performance for two reasons. First, the additional superheating of the vapor causes a decrease in suction density which lowers the refrigerant mass flow and reduces the volumetric capacity. Second,

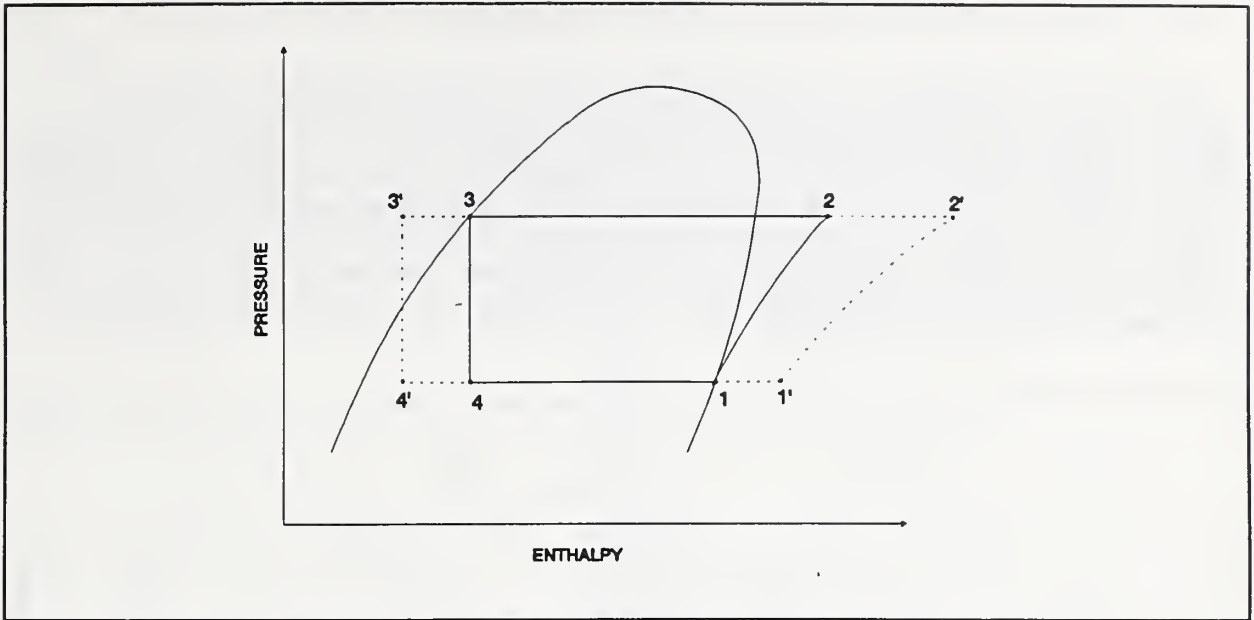


Figure 5 P-H Diagram for Basic and Liquid-Suction Heat Exchange Cycles

the isentropes become flatter (or sloped more to the right) as you move further out into the superheat region. This implies that for an isentropic compression process the enthalpy change for process line 1'-2' will be greater than that of line 1-2. The change in enthalpy for the compression process equals the required work input for that process. The end result is that the work of compression per unit mass of refrigerant circulated will be greater for the modified cycle.

The liquid-suction heat exchanger will increase cycle efficiency if the increase in capacity is larger than the increase in compressor work. Conversely, cycle efficiency will decrease if the increase in compressor work is greater than the increase in capacity. A theoretical derivation of the factors affecting whether or not a liquid-suction heat exchanger benefits an ideal cycle is given in reference [1]. Reference [1] shows that the theoretical performance change produced by a liquid-suction heat exchanger is determined by both the fluid properties and the temperature lift of the application.

### C. Two phase liquid-suction heat exchange

A variation of the liquid-suction heat exchanger cycle can be obtained by operating the system so that two phase refrigerant enters the low pressure side of the liquid-suction heat exchanger. Flooding liquid into the heat exchanger subcools the high pressure refrigerant leaving the condenser with the high quality portion of the phase change. Consider the cycle operated so that the fluid exiting the liquid-suction heat exchanger is saturated vapor. The pressure-enthalpy diagram for this cycle is shown superimposed on the basic cycle in Figure 6.

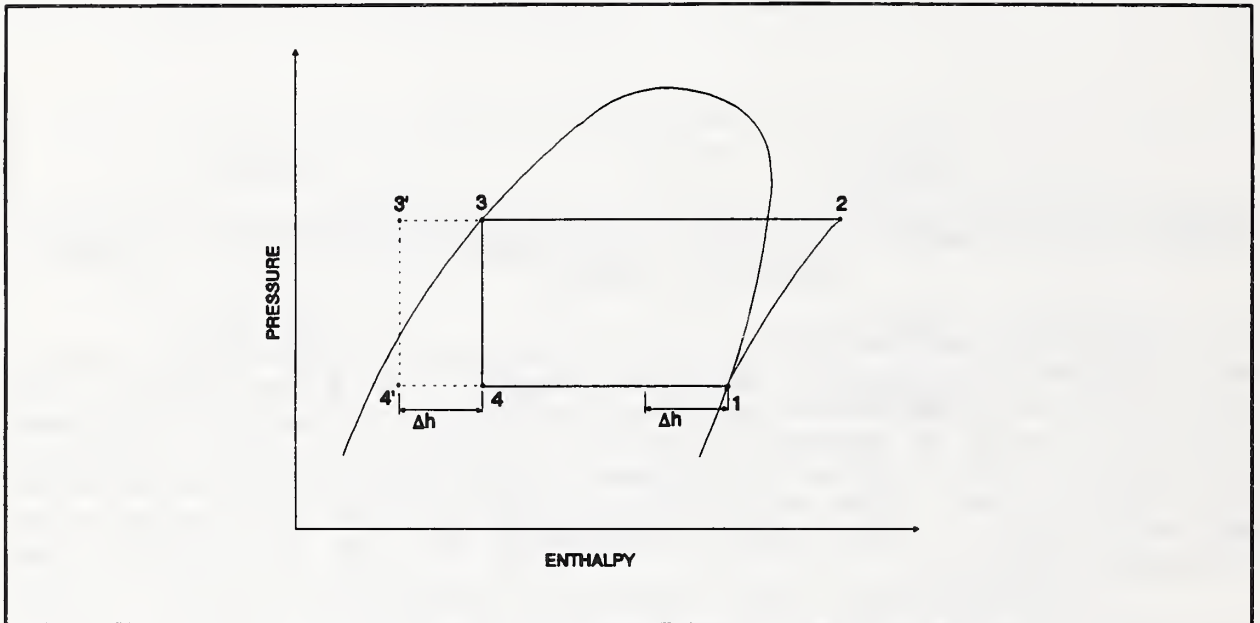


**Figure 6** P-H Diagram for Two-Phase Liquid-Suction Heat Exchange Cycle

In Figure 6, the subcooling of the liquid refrigerant from state point 3 to 3' causes the evaporator entering quality to decrease from 4 to 4'. This produces a rise in the latent heat available for producing a useful refrigerating effect. Unlike the single phase liquid-suction heat exchanger cycle, there is no superheating of the suction vapor. All of the heat removed from the high pressure liquid is added to the end of the vaporization process. The latent heat available for producing useful refrigeration effect is reduced on the right side of the dome by the same amount that it was increased on the left. Consequently, there is no net increase in capacity. Since the state points entering and leaving the compressor (points 1 and 2) have not changed, the work of compression is also unchanged from the basic cycle. Since neither capacity nor compression work has changed from the basic cycle, the ideal COP of the two-phase liquid-suction

heat exchanger cycle would appear to be the same as the ideal basic cycle.

Although this modification produces no theoretical or ideal cycle efficiency change for single component working fluids, for zeotropic mixtures the modification does have an effect. The temperature-entropy graph for the pure fluid is shown in Fig.7, and for the zeotropic mixture in Fig. 8. For the pure fluid the evaporating temperature is a function of the pressure only. Since

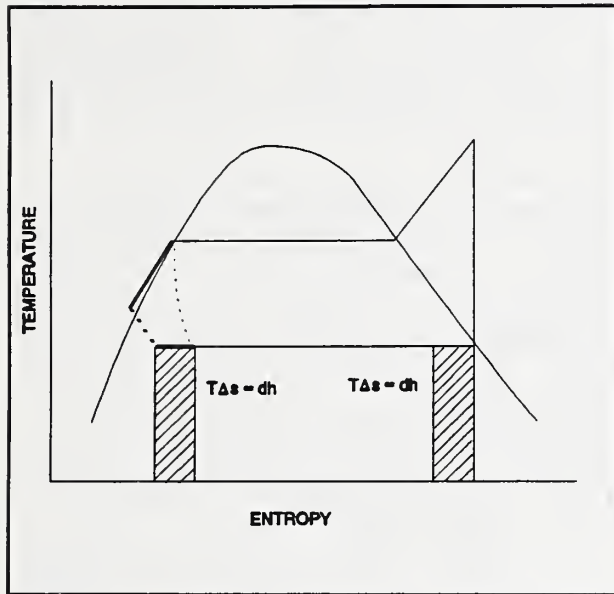


**Figure 7** T-S Diagram for Pure Fluid Two-Phase Liquid-Suction Heat Exchange

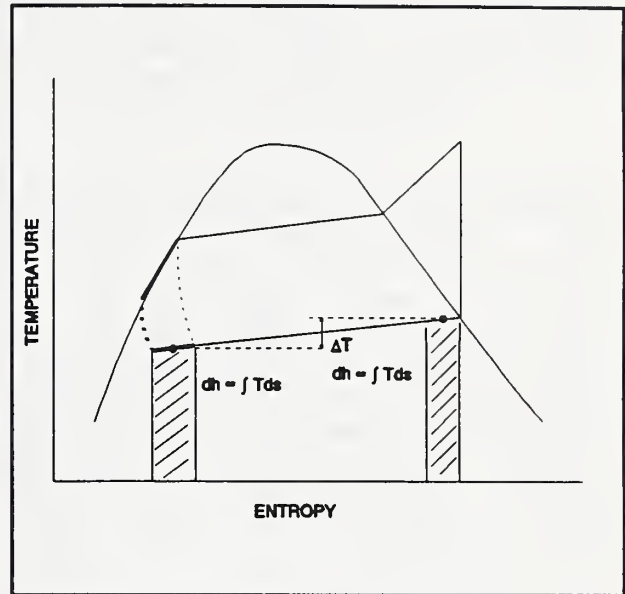


**Figure 8** T-S Diagram for Zeotropic Mixture Two-Phase Liquid-Suction Heat Exchange

the ideal evaporation process occurs along an isobar, as shown in figure 6, the evaporation temperature is also constant. However, for a zeotropic mixture the isobaric vaporization process involves a change in temperature due to the preferential evaporation of the more volatile component. That is, since the composition of the remaining liquid is continuously changing, the evaporating temperature is also changing. The mixture's variable temperature phase change is referred to as the temperature glide.

In Figures 7 and 8 the enthalpy changes ( $dh$ ) on both sides of the dome are equal. However, Figure 8 shows that for a zeotropic mixture the average temperatures of the enthalpy increments are not equal. Therefore, for a mixture the two phase liquid-suction heat exchanger has resulted in a trade of high quality-high temperature fluid for low quality-low temperature fluid. In other words, the average temperature of the vaporization process has been reduced without reducing the vaporization pressure. Assuming the refrigeration system would establish its refrigerant flow rate such that the capacities of both systems were the same, then the average

temperature differences between the respective refrigerants and sensible fluids (i.e., air or water) would be the same, but the mixture would be at a higher evaporator pressure thus, reducing the compressor work [4]. An additional benefit of this cycle modification is that the evaporator effectiveness will be enhanced because the entire heat exchanger will be exposed to two-phase refrigerant.

## DROP-IN TEST PROCEDURE

A drop-in refrigerant, by definition, should require only minor equipment changes that can be accomplished in the field and give performance similar to the refrigerant that it is replacing. For a residential system, such as the one tested, replacement (or readjustment) of the expansion device would be the only system hardware modification that would be considered minor. Since the mass of the drop-in refrigerant charge is not a hardware modification, it will also be varied to optimize the system performance. The following test procedure was developed to optimize system performance (i.e., COP) for each refrigerant within the previously outlined context of a drop-in refrigerant.

In cooling mode, the optimum performance point was determined by finding the charge and valve setting combination that produced the highest efficiency at the 35°C (95°F) rating point. The results of this process are shown for pure R22 and for the mixture in Figures 9 and 10, respectively. In all tests used to produce these figures, the refrigerant charge was adjusted to give the desired value of subcooling, while the expansion valve was adjusted to keep between 1.67 and 2.78°C (3-5°F) of superheat leaving the indoor coil. By adjusting the valve for a minimum of superheat leaving the indoor coil, the highest capacity was obtained, thereby optimizing the performance for each value of subcooling. Figures 9 and 10 show that the optimum values of subcooling were approximately 5.56°C (10°F) for R22 and 2.78°C (5°F) for the mixture. Once the optimum value of subcooling was found, the 27.8°C (82°F) degree cooling test was performed at the same expansion valve setting and refrigerant charge.

Assuming that most residential heat pumps would have two fixed area expansion devices, one for heating and one for cooling, it would seem reasonable to readjust the expansion valve for the heating mode. However, simply readjusting the expansion valve with the same refrigerant charge mass, may or may not produce the best possible performance in heating mode. Therefore, the refrigerant charge was varied in heating mode and performance was optimized exactly as was done in the cooling mode. In practice, a manufacturer can accommodate a different optimum refrigerant charge between the two modes by the strategic allocation of system volume. For example, a line that has no heat transfer but contains vapor in one mode and liquid in another can accommodate the excess charge between the two modes.

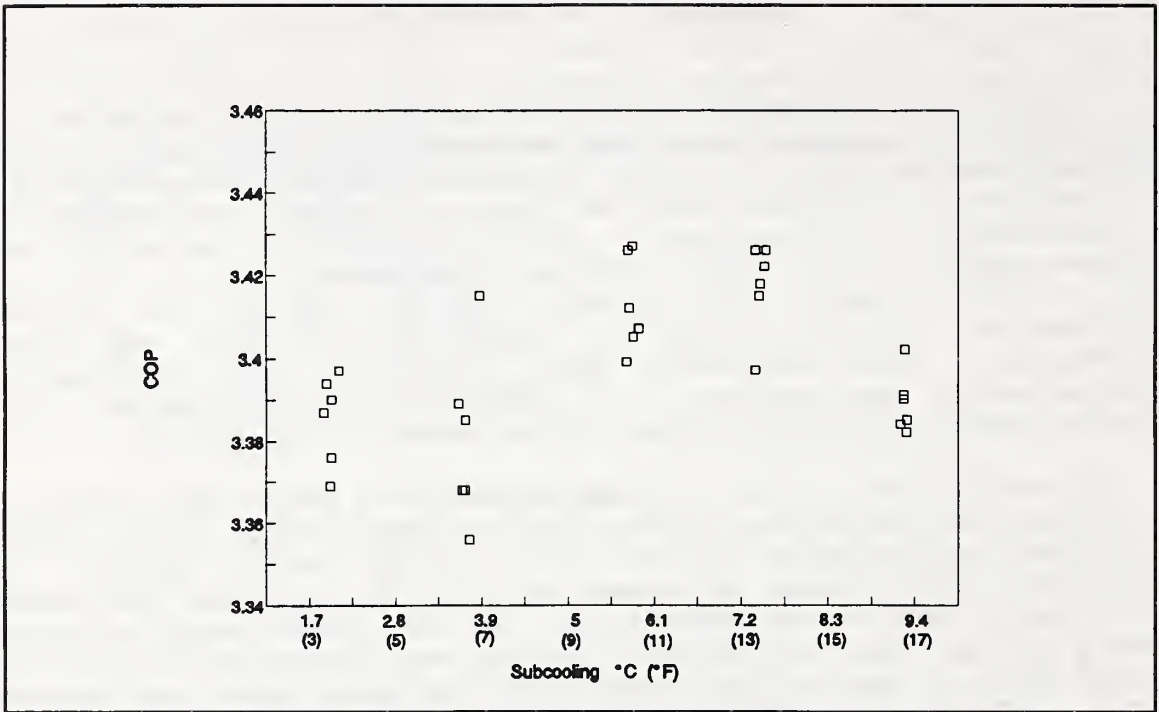


Figure 9 R22 Cooling Mode Charge Optimization at the 35°C (95°F) Rating Point

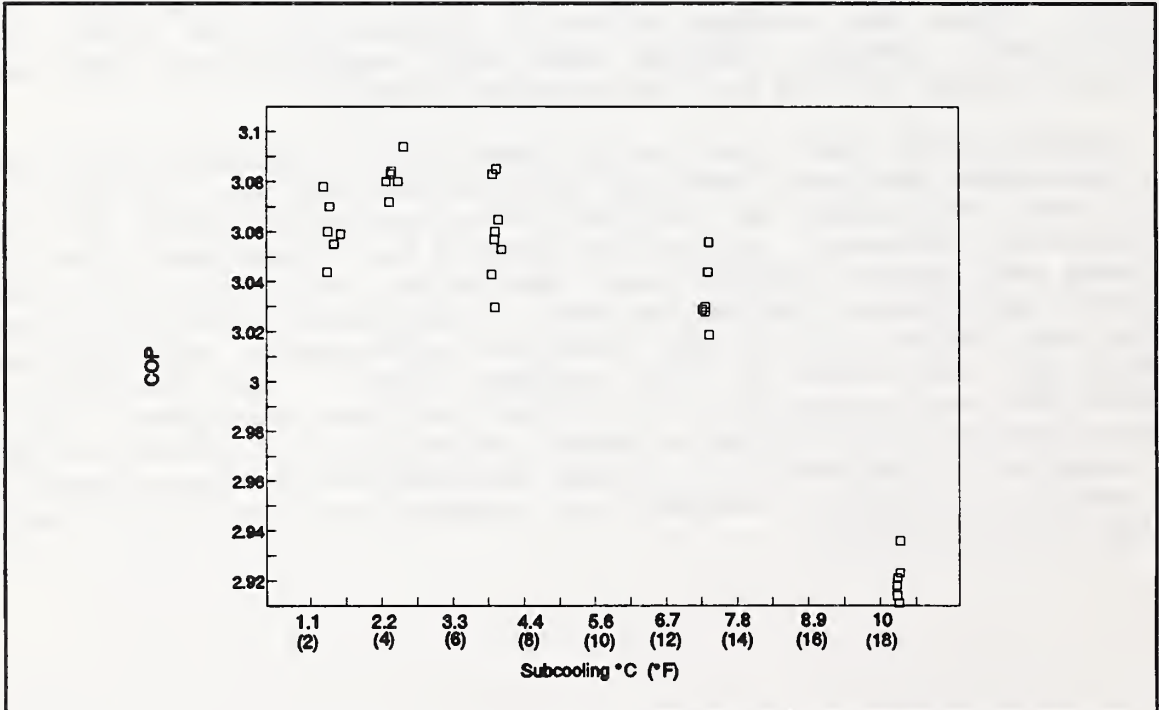
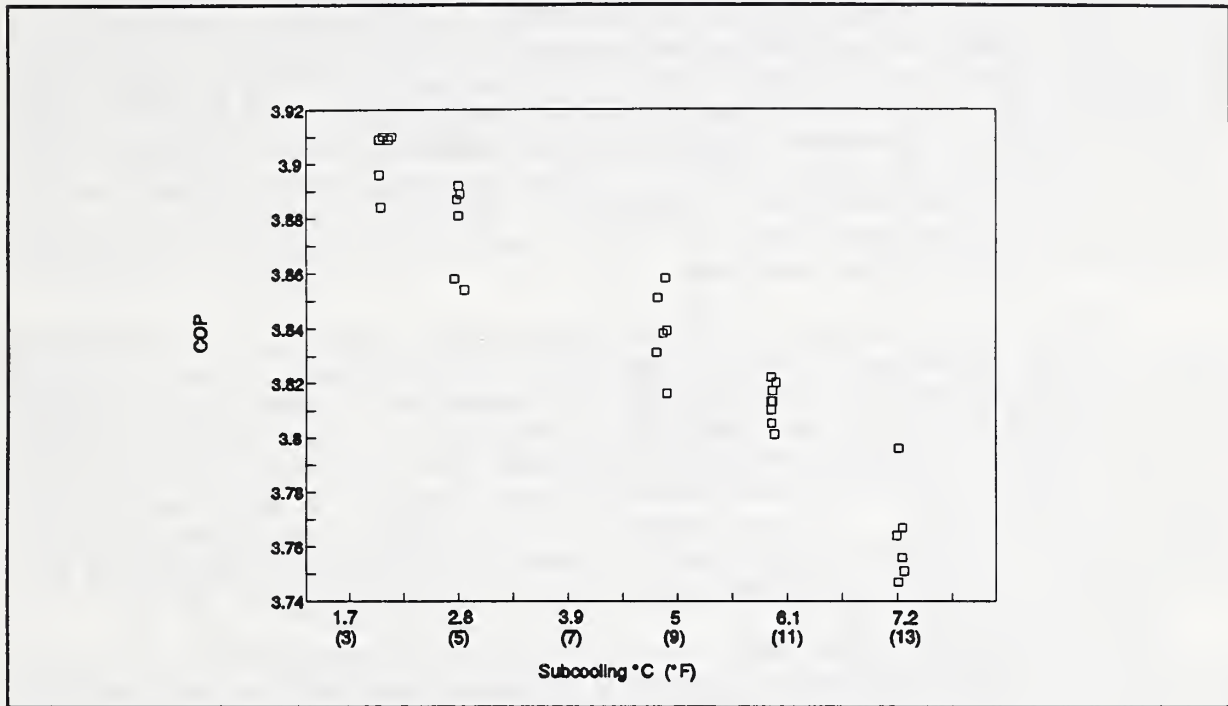


Figure 10 34% R32/66% R134a cooling mode charge optimization at the 35°C (95°F) rating point

The heating mode optimum performance point was determined at the 8.33°C (47°F) degree rating point by adjusting the valve to produce a minimum of superheat while adjusting the refrigerant charge to produce different amounts of subcooling. The results of the heating mode optimization procedure for R22 are shown in Figure 11. The figure shows that the relationship between subcooling and COP is not the same for the heating mode as for the cooling mode. The figure does not display the same type of maximum-minima relationship that was seen in cooling mode.



**Figure 11** R22 Heating Mode Optimization of Charge and Expansion Valve Setting at the 8.33°C (47°F) Rating point

Clearly the maximum COP in Figure 11 would occur if the refrigerant was leaving the condenser at the saturation point. However, it is impractical to operate a system in this manner because all subcooling would be lost for a small drop in outdoor temperature. Consider a system with a constant area expansion device operating in the heating mode at steady state conditions. As the outside temperature falls, the evaporator temperature and pressure will decrease commensurately. Since the indoor temperature remains relatively constant, the high side pressure will also remain relatively constant. Therefore, the compressor will pump less refrigerant due to the lower suction vapor density and increased compression ratio. However, the expansion device will continue to pass the same amount of refrigerant if it is insensitive to changes in low side conditions (i.e., choked flow condition) [5]. Because the expansion device is now passing more

refrigerant than the compressor is pumping, the refrigerant will migrate to the low pressure side of the system where it will collect in the suction accumulator. As the refrigerant migration proceeds the condenser will contain progressively less liquid. The migration of refrigerant cannot proceed indefinitely, so the system must adjust itself to achieve a new steady state. Fortunately, the expansion device mass flow rate is directly proportional to the high-side pressure and the liquid subcooling. The high-side pressure has remained constant, but the liquid subcooling is determined by the amount of liquid in the condenser. Therefore, as the condenser is depleted of liquid the system loses subcooling. Since the amount of refrigerant passed by the expansion device is directly proportional to the amount of subcooling, the gradual loss of subcooling causes a gradual decrease in the expansion device mass flow rate. When the expansion device mass flow becomes equal to the compressor mass flow, a new steady state equilibrium condition will be reached. This new equilibrium condition will have less subcooling and may even have two phase refrigerant entering the expansion device.

Since any refrigerant that leaves the condenser in the vapor state cannot produce a useful refrigerating effect, the complete loss of subcooling is undesirable. Therefore, operating a system with saturated liquid leaving the condenser at the  $8.33^{\circ}\text{C}$  ( $47^{\circ}\text{F}$ ) heating condition would cause an extreme loss of subcooling at the  $-8.33^{\circ}\text{C}$  ( $17^{\circ}\text{F}$ ) heating condition. This would be detrimental to system performance. Since there was no clear point of optimum performance in heating mode, the expansion valve was adjusted for a practical minimum of subcooling.

As previously described, the "drop-in" procedure was designed to optimize the machinery for each refrigerant within the limits allowed by the drop-in definition (i.e., changes in charge mass and expansion valve setting only). In this context, optimization of the machinery implies that the refrigerant charge be adjusted to find the point of maximum COP. Changing the refrigerant charge causes changes in the COP by affecting the liquid subcooling and the cycle temperature lift. For example, a minimal amount of subcooling causes a high evaporator entering quality. This reduces the latent heat of vaporization available to produce a useful refrigerating effect. Consequently, the capacity and COP are both penalized. As the subcooling is increased the evaporator entering quality is decreased. This allows a greater portion of the latent heat of vaporization to produce a useful refrigerating effect. This will cause both capacity and COP to increase. However, increasing the subcooling also produces a concurrent rise in condenser pressure. The condenser pressure increases because a greater fraction of the condenser surface area becomes dedicated to subcooling the liquid. Consequently, there is less surface area available to reject the vapor superheat and the latent heat of condensation. Since the condenser UA value and entering air temperature are constant, the average condensing temperature and

pressure will rise. Since the low-side pressure remains practically constant, the result is an increased compression ratio and cycle temperature lift. This causes the refrigerant mass flow to go down and the compression work per pound of refrigerant circulated to go up. Both of these factors will produce reductions in capacity and COP. In summary, increases in subcooling produce two competing effects; a greater available latent heat increases the COP, while the increased condenser pressure reduces it.

Although Figures 9, 10 and 11 were all produced by the same optimization procedure, they each have distinctly different functional relationships between COP and degree of subcooling. The capacity and power input are shown for the optimization process as functions of the subcooling in Figures 12 and 13, respectively. Each curve in these figures corresponds to one of the optimization

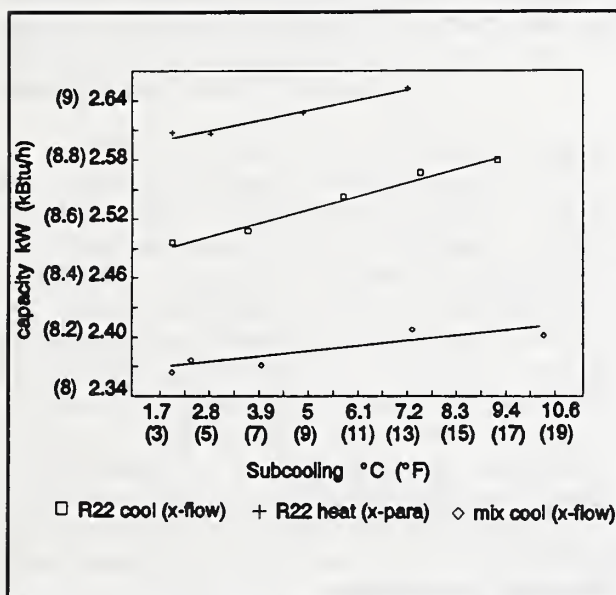


Figure 12 Variation of Capacity With Subcooling

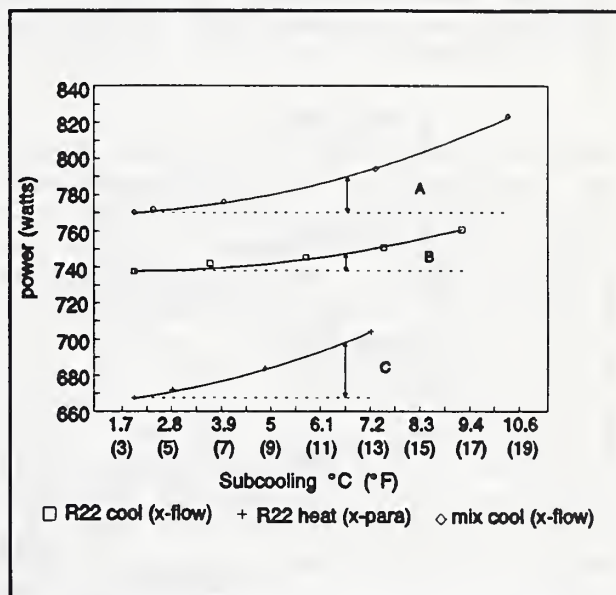


Figure 13 Variation of Power With Subcooling

curves shown in Figures 9, 10 and 11. In Figures 12 and 13 the notations in parenthesis refer to the heat exchange configuration of the condenser. Specifically, "x-flow" refers to crossflow and "x-para" refers to a cross-parallel flow configuration. In all cases the capacity increase is a linear function of the subcooling, but the compression work or power input is a non-linear function of the subcooling. As stated previously, an increase in subcooling produces two competing effects; capacity is increased due to lower evaporator entering quality and compression work is increased due to the larger compression ratio. The shape of the COP optimization curve ultimately depends on the relative magnitude of these two effects.

Since the capacity and power are respectively linear and non-

linear functions of the subcooling, the shape of the optimization curve will be most strongly influenced by the power. Considering the cooling mode, Figure 13 shows the mixture to have a greater power increase for an equivalent amount of subcooling. This fact is illustrated by the relative lengths of line segments A and B. If we recall the expression for the compression work per unit mass (Equation 11) and recognize that  $P_g$  and  $v_g$  are constant for each optimization curve, we see that the power increase is determined solely by the ratio  $P_d/P_g$ . Therefore, we can replace Figure 13 with a plot of the condenser pressure against the subcooling as shown in Figure 14. Further evidence that the pressure increase is solely responsible for the power increase comes from the fact that Figures 13 and 14 have identical shapes.

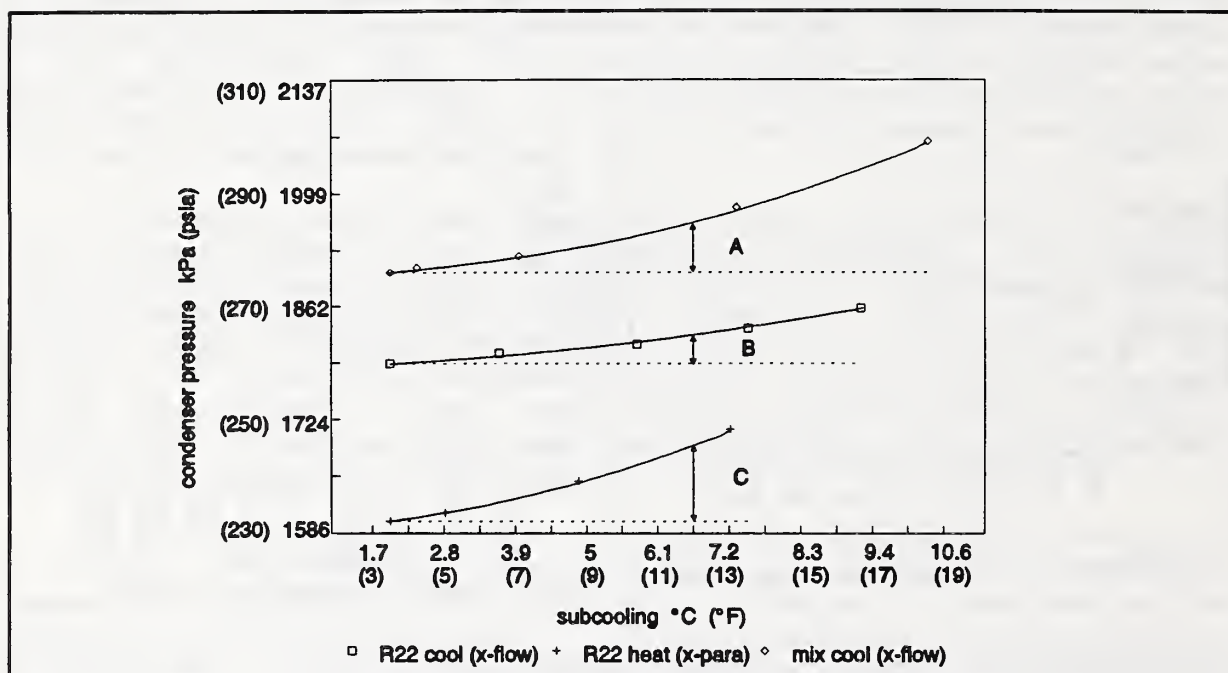


Figure 14 Variation of Condenser Pressure With Subcooling

The motivation for substituting the pressure increase versus subcooling (Fig. 14) for the power increase (Fig. 13) is that the pressure change with subcooling can be easily explained on the basis of the  $\ln(P)$  vs.  $(-1/T)$  graph for the two fluids. Referring to Figure 2, the mixture has a greater slope than R22. Therefore, an equal increase in condensing temperature will produce a greater pressure increase for the mixture than for R22. Similar to Figure 13, the pressure changes for equivalent amounts of subcooling are shown in Figure 14 by the relative lengths of line segments A and B. In summary, the larger slope of the pressure-temperature relationship of the mixture relative to R22 causes a faster rise in condenser pressure (and thus compressor power) as the subcooling is increased. Therefore, as shown in Figures 9 and 10 the mixture shows a sharper COP peak at lower values of subcooling than R22.

In heating mode, the optimization curve shown in Figure 11 has no optimum point as in Figures 9 and 10. The reason for this is that the optimization procedure was designed to hold low-side parameters (pressure and superheat) fixed while the high-side parameters (pressure and subcooling) were varied. Therefore, the process is only sensitive to the fluid properties and the heat exchange configuration of the condenser. In a given mode (heating or cooling), the condenser configuration is the same for both fluids. Therefore, the different optimization curve shapes were determined by the difference in fluid properties. However, when the operating mode is switched from cooling to heating the condenser configuration is different. In the cooling mode, the nearly pure crossflow outdoor coil serves as the condenser. Whereas, in heating mode, the cross-parallel flow indoor coil (which was a cross-counter flow evaporator in the cooling mode) serves as the condenser. Since Figures 9 (R22 cooling mode) and 11 (R22 heating mode) are for the same fluid, the lack of an optimum point in Figure 11 must be attributed to the difference in condenser configuration.

The effect of condenser configuration can be easily understood by considering what happens in the condenser as subcooling is increased. As refrigerant is added to increase the subcooling, progressively more of the condenser volume becomes occupied with liquid. For all types of heat exchanger geometries this cuts down on the surface area available for condensation and causes the condensing temperature and pressure to rise. Additionally, since the last portion of the heat exchanger now has a single phase fluid on both sides (air and refrigerant liquid) the temperatures of the two fluids will approach each other. If the heat exchanger is crossflow the refrigerant will always approach the same entering air temperature. If the heat exchanger is cross-parallel flow, the refrigerant liquid will approach the leaving air temperature. Since the leaving air has already picked up the heat of condensation from the refrigerant its temperature will be higher than the entering air. Since increased subcooling causes both the capacity and the rejected heat to be higher, the leaving refrigerant liquid will approach a higher air temperature for higher values of subcooling. Consequently, for an equal increase in subcooling the increase in compressor power and condenser pressure will be larger for a cross-parallel flow condenser than a crossflow condenser. This fact is illustrated in Figures 13 and 14 by the length of line segment C.

The magnitude of the condenser pressure rise associated with increased subcooling has been shown to be determined by both fluid properties and the heat exchange configuration of the condenser. Separate cases have been identified where an increase in subcooling either increased or decreased the COP, and if it existed an optimum amount of subcooling was found. The relationship between subcooling and COP can be changed with the addition of a liquid-suction heat exchanger. For example, at the 47°F heating condition the cross-parallel condenser causes the point of optimum COP to

occur with saturated liquid leaving the condenser (see Fig.11). However, it was previously pointed out that it is impractical to operate the system with no subcooling at this condition. With a liquid-suction heat exchanger subcooling can be accomplished outside of the condenser so that there is no performance penalty caused by increased condenser pressure. However, this does imply that as the outside temperature falls refrigerant will be condensing in the liquid-suction heat exchanger. The ramifications of this must be considered.

In cooling mode, the liquid-suction heat exchanger can also be used to produce subcooling outside of the condenser. Similar to heating mode, the refrigerant can then be allowed to leave the condenser as a saturated liquid. The result will be a lower average condensing temperature. Performing all of the subcooling in a liquid-suction heat exchanger may or may not increase COP since there are other factors involved (see section on liquid-suction heat exchange).

## DROP-IN TEST RESULTS

The cooling mode test results are shown in Table 1 for both R22 and the mixture. The heating mode test results are shown in Table 2. It should be noted that the discharge line temperatures in Tables 1 and 2 are unusually low for the  $-8.33^{\circ}\text{C}$  ( $17^{\circ}\text{F}$ ) heating test, which would ordinarily have the highest discharge line temperature. These low discharge line temperatures result from the large compressor shell heat loss that is characteristic of the compressor used in this study. The compressor manufacturer indicated that the compressor was designed with high side motor cooling. Additionally, the flow of discharge gas was configured so that the compressor shell would act as an internal oil separator. The combination of these two factors increases the potential for heat transfer between the discharge gas and the compressor shell. Since the relevant heat transfer modes between the shell and the environment (natural convection and radiation) are both proportional to the temperature difference between the shell and the environment, the total heat loss from the discharge gas is also directly proportional to this temperature difference. This implies that a discharge temperature which is measured outside of the compressor shell, is not necessarily representative of the temperature at the discharge valve. Although more representative discharge temperatures could have been obtained by increasing the insulation on the compressor shell, caution was exercised to avoid overheating the motor.

The large compressor shell heat loss present in this apparatus also complicates the taking of composition samples from the discharge line. As can be seen in Table 2, the refrigerant in the discharge line is in a state of saturation for the  $-8.33^{\circ}\text{C}$  ( $17^{\circ}\text{F}$ ) heating mode tests. (This is probably due to condensate forming on the relatively cool line walls). If a composition sample were taken here, it could be incorrect due to the composition difference between the liquid and vapor phases of a refrigerant mixture. This problem was circumvented by electrically heating a section of the discharge line to insure that the sample was drawn from superheated refrigerant.

A summary of the mixture performance relative to that of R22 at the four rating points is shown in Table 3. The values in this table are normalized by the R22 results for the same test. The capacity for the rating points of both R22 and the mixture are also presented graphically in Figure 15. This figure clearly shows the capacity increase of the mixture due to the passive composition shift at the  $-8.33^{\circ}\text{C}$  ( $17^{\circ}\text{F}$ ) heating test.

TABLE 1. COOLING MODE TEST RESULTS

OUTDOOR TEMP. °C (°F)	CAPACITY W (Btu/h)			POWER INPUT W	COP (EER) (Btu/W*h)	COMP. BY WEIGHT	REFRIG. PRESS. kPa (psia)		DISCH. LINE TEMP °C (°F)
	SENS	LAT	TOTAL				DISCH.	SUCT.	
35 (95)	1918 (6545)	637 (2175)	2555 (8720)	743.3	3.437 (11.728)	PURE R22	1824 (264.5)	618 (89.7)	88.9 (192.0)
27.8 (82)	1932 (6593)	744 (2540)	2676 (9133)	643.3	4.159 (14.191)	PURE R22	1541 (223.5)	586 (85.0)	88.8 (191.8)
35 (95)	1843 (6287)	533 (1819)	2736 (8106)	776.3	3.059 (10.438)	34.06% R32	1927 (279.5)	561 (81.3)	91.9 (197.5)
27.8 (82)	1883 (6425)	641 (2186)	2524 (8611)	672.3	3.753 (12.806)	34.06% R32	1621 (235.1)	536 (77.7)	87.7 (189.8)

Note: The uncertainty in the measured cooling capacity was calculated to be 2.5% (see Appendix B).

TABLE 2. HEATING MODE TEST RESULTS

OUTDOOR TEMP. °C (°F)	CAPACITY W (Btu/h)	POWER INPUT (W)	COP	COMP. BY WEIGHT	REFRIG. PRESS.		DISCH LINE TEMP °C (°F)
					kPa DISCH.	(psia) SUCT.	
8.33 (47)	2668 (9103)	699.6	3.812	PURE R22	1713 (248.4)	510 (73.9)	84.9 (184.9)
-8.33 (17)	1325 (4520)	545.8	2.426	PURE R22	1250 (181.3)	319 (46.2)	32.1 (89.8)
8.33 (47)	2474 (8441)	716.5	3.452	33.96% R32	1790 (259.6)	454 (65.9)	86.2 (187.2)
-8.33 (17)	1381 (4712)	630.6	2.189	35.55% R32	1416 (205.4)	316 (45.9)	36.9 (98.4)

Note: The uncertainty in the measured heating capacity was calculated to be 2.4% (see Appendix A).

**TABLE 3. NORMALIZED PERFORMANCE VALUES**

TEST CONDITION °C (°F)	NORMALIZED CAPACITY	NORMALIZED COP	NORMALIZED POWER
COOLING 35 (95)	0.930	0.890	1.044
COOLING 27.8 (82)	0.943	0.902	1.045
HEATING 8.33 (47)	0.927	0.906	1.024
HEATING -8.33 (17)	1.042	0.902	1.155

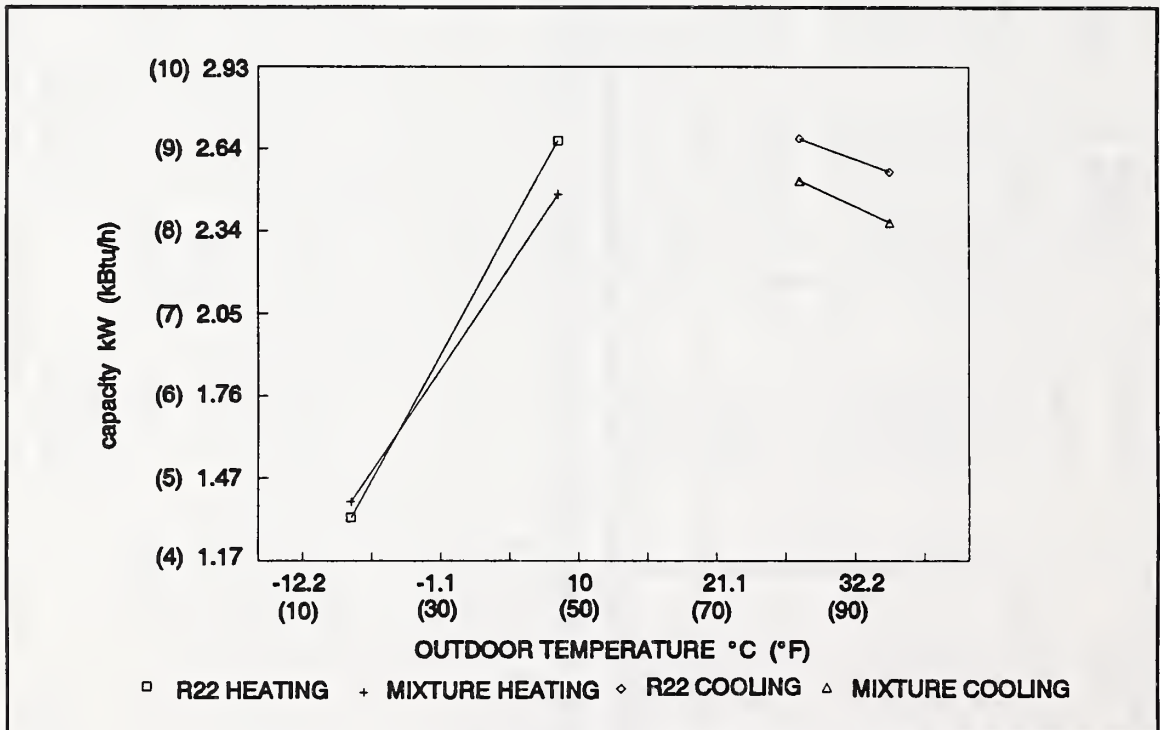


**Figure 15 Capacity at the rating points for R22 and the mixture**

## ANALYSIS OF DROP-IN TEST RESULTS

Based on the normalized test results shown in Table 3, the mixture test composition of 34% R32 and 66% R134a by weight will yield a lower capacity and COP than the R22 it is replacing in this system. From an equipment owner's standpoint, a drop in COP would present an economic burden due to increased operating costs. Although this is undesirable, it would have the advantage of not requiring replacement of the equipment. However, a similar loss in capacity may be intolerable if the equipment no longer meets the load.

The reason for the mixture's lower capacity can be explained on a theoretical basis by examining the product of suction density and the available enthalpy (or latent heat) of vaporization. The available latent heat represents the amount of refrigeration effect produced per pound of refrigerant circulated, and the suction density is a measure of the refrigerant circulated per unit volume of compressor displacement. The product of these two quantities, which has units of  $\text{kJ/m}^3$  ( $\text{Btu/ft}^3$ ), represents the volumetric capacity of the refrigerant. The  $35^\circ\text{C}$  ( $95^\circ\text{F}$ ) cooling mode values of this product, for R22 and the mixture, are shown in Table 4. Table 4 also shows the suction density at the compressor inlet and the available enthalpy of vaporization. The available enthalpy of vaporization is calculated by assuming an isenthalpic expansion. Table 4 shows the ratio of the mixture capacity to the R22 capacity from the test data to be nearly the same as that calculated from the available latent heat suction density product. The excellent agreement between these two ratios suggests that the product of available latent heat and suction density is a good measure of a refrigerant's theoretical capacity potential at a given evaporator pressure.

Further comparisons between the two refrigerants performance in this system can be facilitated by plotting both cycles on P-H coordinates. A P-H diagram for the  $35^\circ\text{C}$  ( $95^\circ\text{F}$ ) cooling test is shown for R22 and the mixture in Figure 16. This figure shows that the pressure lift of the mixture cycle is considerably higher. Figure 16 dramatically points out that the mixture has a latent heat of vaporization much greater than R22. Considered by itself, the higher latent heat would indicate that the mixture should have a higher capacity. However, the test data shows that R22 has a higher capacity. This fact again reinforces the importance of considering the product of latent heat and suction density, as the primary measure of a refrigerant's volumetric capacity.

It is instructive to plot both the R22 and the mixture cycles on T-S coordinates. A T-S diagram for the 35°C (95°F) cooling test is shown for R22 and the mixture in Figure 17. A comparison of the P-H and T-S diagrams reaffirms what was previously shown from  $\ln(P)$  vs.  $(-1/T)$  diagrams; for equal average condensing temperatures the mixture will have a higher discharge pressure.

**TABLE 4**  
**REFRIGERANT CAPACITY POTENTIAL: 35°C**  
**(95°F) COOLING MODE PERFORMANCE COMPARISON**

35°C (95°F) COOLING	R22	34% R32 66% R134a
TOTAL CAP. W (BTU/H)	2556 (8720)	2376 (8106)
SENS CAP. W (BTU/H)	1918 (6545)	1843 (6287)
LATENT CAP. W (BTU/H)	637 (2175)	533 (1819)
LATENT FRACTION	0.249	0.224
POWER (W)	743.3	776.3
COP	3.437	3.059
(Q MIX)/(Q R22)	0.930	
(POWER MIX)/(POWER R22)	1.044	
(COP MIX)/(COP R22)	0.930	
DISCH PRESS kPa (PSIA)	1824 (264.5)	1927 (279.5)
SUCT PRESS kPa (PSIA)	618 (89.7)	561 (81.3)
DISCH/SUCT	2.949	3.438
SUBCOOLING °C (°F)	5.7 (10.2)	4.4 (7.9)
SUPERHEAT °C (°F)	1.6 (2.9)	4.2 (7.5)
SUCT DENSITY $\rho$ kg/m <sup>3</sup> (LB/FT <sup>3</sup> )	24.5339 (1.5316)	19.3295 (1.2067)
REFRIGERANT $\Delta h$ kJ/kg (BTU/LB)	159.96 (68.77)	186.75 (80.29)
$\rho \cdot \Delta h$ kJ/m <sup>3</sup> (BTU/FT <sup>3</sup> )	3924.44 (105.328)	3609.78 (96.886)
PERFORMANCE POTENTIAL (MIX $\rho \cdot \Delta h$ )/(R22 $\rho \cdot \Delta h$ )	0.920	
CALCULATED REF. MASS FLOW RATE kg/min (LB/MIN)	0.957 (2.11)	0.762 (1.68)

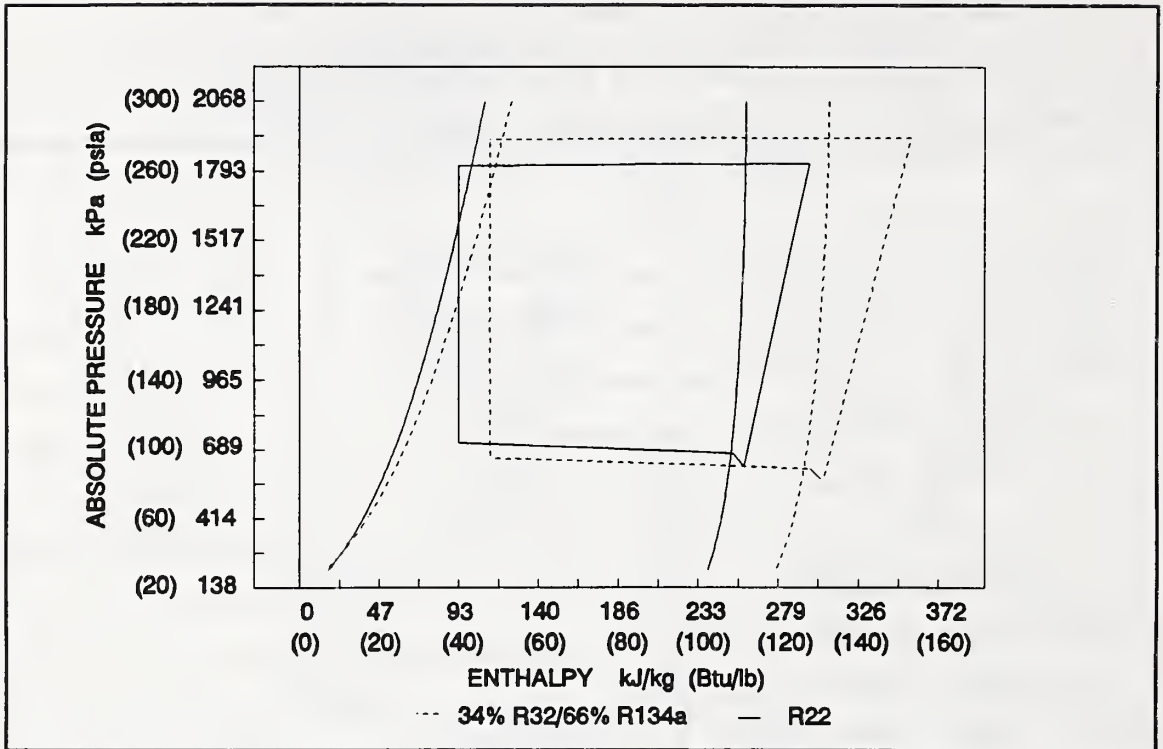


Figure 16 P-H diagram for R22 and 34% R32/66% R134a

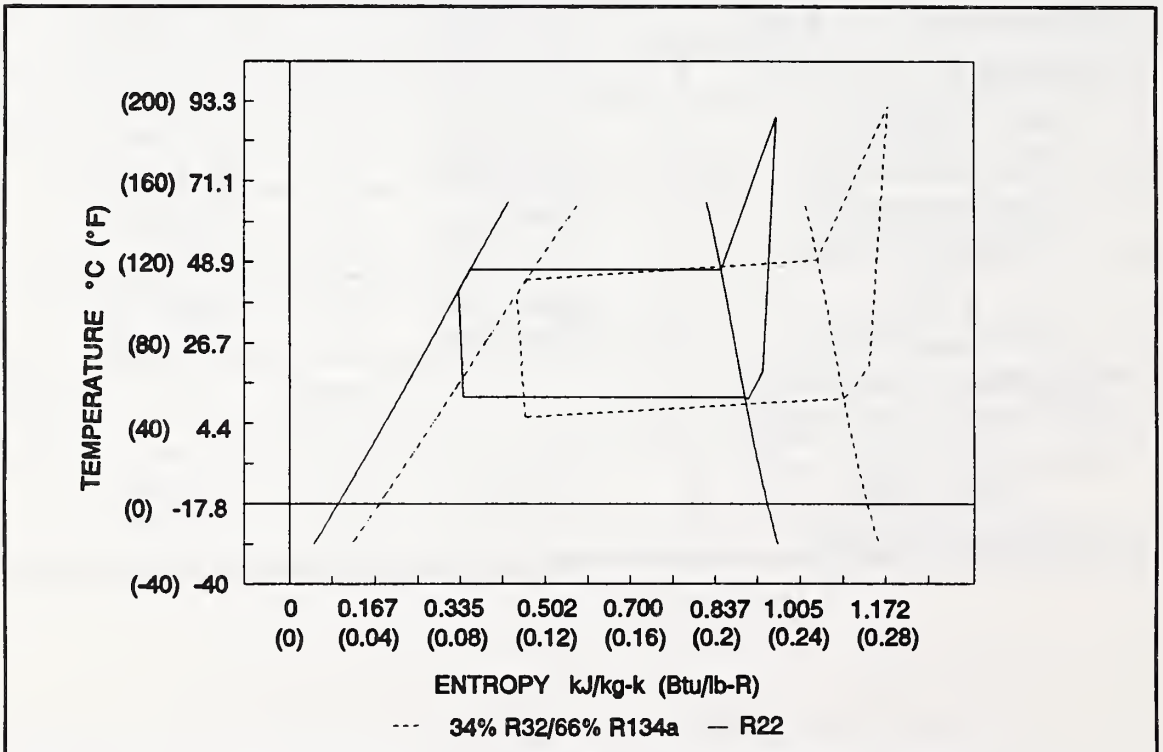
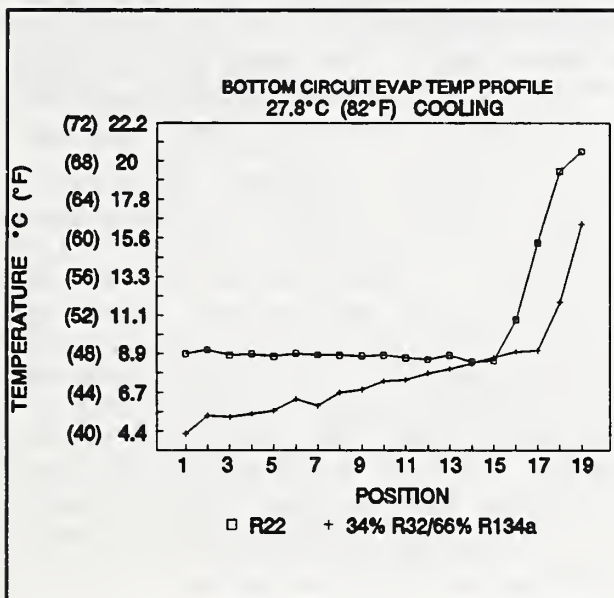


Figure 17 T-S Diagram for R22 and 34% R32/66% R134a

Although the fluid properties of the mixture produced a lower capacity and COP than R22 at the operating conditions shown in Table 4, there are certain aspects of the test procedure that produced conditions somewhat biased against the mixture. For example, Table 4 shows that the optimized test superheat was 1.6°C (2.9°F) for R22 and 4.2°C (7.5°F) for the mixture. The additional superheat of the mixture test decreased the capacity and increased the work of compression. Consequently, the mixture refrigerant charge was not as well optimized for the machine as was the R22 charge. The additional superheat imposed on the mixture test was a result of inaccuracies in the thermodynamic property program. A subsequent version of the property program which was able to correctly represent R32 mixtures was received after testing was completed. It was unknown at the time of testing that the superheat was higher for the mixture.

Another aspect of the test procedure which tends to penalize the mixture performance was the decision to adjust the expansion valve for equal amounts of superheat. With this valve adjustment criterion, the mixture's temperature glide causes it to have a lower average evaporator temperature than R22. The lower average evaporator temperature of the mixture is evident in the T-S diagram (Figure 17) and in the evaporator temperature profiles for the 27.8°C (82°F) cooling test which are shown in Figures 18 and 19. The 27.8°C (82°F) cooling test was selected for these figures



**Figure 18 Cooling Mode  
Bottom Circuit Evaporator  
Temperature Profiles**

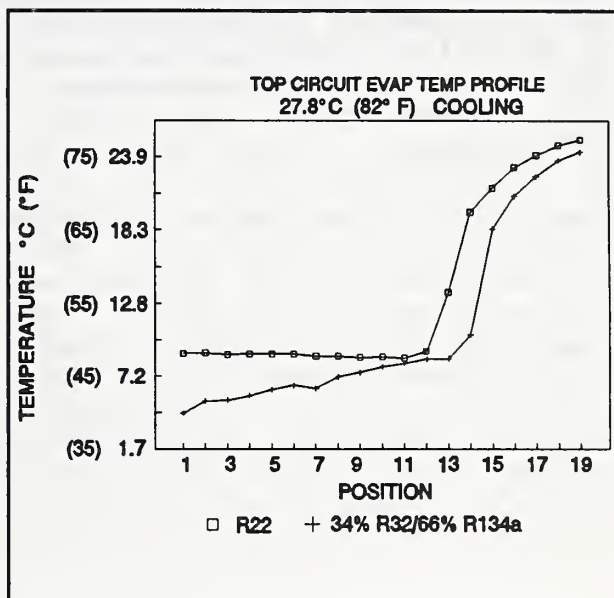


**Figure 19 Cooling Mode  
Top Circuit Temperature  
Profiles**

because the starved evaporator that is characteristic of this test causes the refrigerant to closely approach the entering air temperature. Consequently, both evaporator circuits for each fluid

have approximately the same amount of superheat. The performance penalty caused by the mixture's lower average evaporator temperature is a result of the corresponding lower evaporator pressure. The lower pressure decreases the suction density and increases the compression ratio.

An alternative test procedure would be to adjust the expansion valve to produce the same average saturation temperatures in the evaporator for both the mixture and R22. Assuming that both fluids would leave the evaporator at approximately the same temperature (equal approach temperature), adjusting the valve for equal average saturation temperatures would cause the mixture to have less superheat than the pure fluid. This procedure would give the mixture a higher saturation pressure than it would have if the valve was adjusted for the same superheat as the pure fluid. The higher suction pressure would increase the suction density and decrease the compression ratio. The net result would be to increase the mixture's performance relative to R22. However, this test procedure may be viewed as biasing the results in favor of the mixture.

The bottom line is that the effect of the test procedure and the equipment must be considered when comparing refrigerants in a drop-in context. In a larger sense, it brings into question the whole concept of comparing the performance of any two refrigerants in the same machine and claiming one to be superior to the other. Each refrigerant requires a unique system design if the refrigerant is to achieve its full performance potential. In general, as the vapor pressure and temperature glide of the fluids being compared gets farther apart, the validity of drop-in comparisons becomes more suspect.

## LEGITIMACY OF THE DROP-IN TEST AS A BASIS FOR COMPARING THE TWO REFRIGERANTS

An unbiased method of comparing pure and zeotropic mixed refrigerants was suggested by McLinden and Radermacher [6]. They proposed that refrigerants be compared by holding constant the total UA of both heat exchangers per unit capacity. The effect of this comparison criteria is to have an equal heat flux for each refrigerant compared. To evaluate the validity of the drop-in tests conducted in this study the degree to which this criteria has been satisfied should be examined. However, it was not possible to accurately calculate UA from the experimental data because the air temperature profile through the heat exchanger was unknown, and the assumptions needed for the calculation of a log mean temperature difference were not met (i.e., the specific heat and heat transfer coefficient were not constant).

Because UA could not be accurately calculated from experimental data, a semi-theoretical cycle model developed at NIST called CYCLE11 [7] was used. The program has the capability to simulate both counterflow and crossflow heat exchangers with values for pressure drops, subcooling, superheat and compressor polytropic efficiency specified as inputs. The program considers the expansion process as isenthalpic. Additional inputs are the volumetric displacement of the compressor and the UA value for each heat exchanger. Although the absolute value of the results from an ideal cycle model will not reflect that of lab data, the results can be used on a relative basis.

A demonstration of the ideal cycle model's ability to accurately reflect relative changes in cycle performance is summarized in Table 5. The table shows the experimental and ideal cycle values of capacity, COP and power input normalized by the R22 values for each case. The program results were calculated by inputting the values for pressure drop, subcooling, superheat and temperature change of the air streams (referred to as the heat transfer fluid (HTF) temperature glide) from the experimental data. The program was then iterated with different UA values until the system pressures matched the experimental data. The fact that the computer simulated ratios agreed with the actual data ratios supports the use of the ideal cycle model to forecast relative trends in cycle performance.

**TABLE 5. VERIFICATION OF CYCLE11 AS A TOOL FOR PREDICTING RELATIVE PERFORMANCE TRENDS**

TEST CONDITION AND TYPE	NORMALIZED CAPACITY	NORMALIZED COP	NORMALIZED POWER
LAB DATA COOLING 35°C (95°F)	0.930	0.890	1.044
COMPUTER MODEL COOLING 35°C (95°F)	0.935	0.901	1.038

Since the ideal cycle computer projections have been shown to be reasonable on a relative basis, they can be used to calculate the UA values for the heat exchangers. The results of the calculated UA values for the same program inputs as Table 5 are shown in Table 6. The absolute value of the UA numbers reported in Table 6 are a function of the compressor displacement used in the program. Therefore, it must be stressed that these values are to be interpreted on a relative basis only.

**TABLE 6. CYCLE11 RELATIVE UA CALCULATIONS**

REFRIGERANT	UA evap W/°C (Btu/h-°F)	UA cond W/°C (Btu/h-°F)	UA total/Qe 1/°C (1/°F)
R22	422 (800)	781 (1480)	0.0975 (0.1755)
34% R32 66% R134a	295 (560)	617 (1170)	0.0791 (0.1424)
% DIFFERENCE (R22-MIX)/R22	30.0%	20.9%	18.9%

As shown in Table 6, the large difference in total UA per unit capacity (18.9%) produced by the combination of heat pump and test procedure utilized for this drop-in test biases the results in favor of R22. The test results do not reflect the performance potential of the mixture since the equipment has unduly handicapped the mixture performance. Under these circumstances, the test cannot be considered a fair and valid comparison of the fluids.

The reason for the decreased UA of the mixture should be considered. Since the area (A) and the compressor volumetric displacement were both constant for all tests, the changes must have occurred in the heat conductance (U). For a given internal surface, the factors that affect the value of U are the refrigerant's transport properties, the refrigerant mass flow

(velocity) and the interaction between the refrigerant and the lubricating oil. The refrigerant mass flow is proportional to the suction density and was calculated in Table 4 to be 20.4% lower for the mixture. The effects of the transport property differences and oil interactions are more difficult to characterize and will not be addressed in this report.

## LIQUID-SUCTION HEAT EXCHANGER TESTS

Because of its theoretical potential for performance improvement an additional series of tests were conducted with a liquid-suction heat exchanger. The heat exchanger was a typical off-the-shelf variety, and was installed in the suction line between the indoor coil and the reversing valve. Since the location of the heat exchanger would have to be changed for the heating mode, heat exchanger tests were performed only in the cooling mode. As described previously, there are two possible ways to operate the system with the liquid-suction heat exchanger. The expansion valve can be adjusted so that the low pressure side of the heat exchanger contains single phase vapor only, or the valve can be set so that low pressure liquid refrigerant floods into the heat exchanger. Both types of tests were performed in this study. The performance of the system modified with a liquid-suction heat exchanger normalized by the unmodified R22 performance values are shown in Table 7. The normalized cooling mode values from Table 3 are reproduced for comparison purposes. The symbol  $\phi$  denotes the phase of the low pressure refrigerant entering the liquid-suction heat exchanger. For all the results shown in table 7, except those that are marked with an asterisk, the expansion valve was adjusted at the 35°C (95°F) test condition. For the results marked with an asterisk the expansion valve was adjusted at the 27.8°C (82°F) condition.

**TABLE 7. NORMALIZED PERFORMANCE WITH THE LIQUID-SUCTION HEAT EXCHANGER**

TEST CONDITION AND TYPE °C (°F)		NORMALIZED CAPACITY	NORMALIZED COP	NORMALIZED POWER
35 (95)	NO HX	0.930	0.950	1.044
	HX 1- $\phi$	0.950	0.901	1.054
	HX 2- $\phi$	0.950	0.906	1.055
	* HX 2- $\phi$	0.950	0.906	1.056
27.8 (82)	NO HX	0.930	0.902	1.045
	HX 1- $\phi$	0.906	0.872	1.044
	HX 2- $\phi$	0.916	0.880	1.041
	ADJ. VALVE * HX 2- $\phi$	0.966	0.919	1.051

An interesting aspect of the results shown in Table 7 is that for all tests where the expansion valve was adjusted at the 35°C

(95°F) test condition the performance of the liquid-suction heat exchanger cycle at the 27.8°C (82°F) test condition was worse than the unmodified cycle. The decreased performance at the 27.8°C (82°F) test condition was a result of the test being designed to simulate a fixed area expansion device. Therefore, when the valve was adjusted at the 35°C (95°F) condition no further valve adjustments were made at the 27.8°C (82°F) test condition. For a given fixed area expansion device, the amount of refrigerant fed to the coil is directly proportional to the pressure drop across the valve and the amount of subcooling. In the unmodified basic cycle, when the expansion valve was adjusted at the 35°C (95°F) condition the lower discharge pressure of the 27.8°C (82°F) condition causes the evaporator to be starved. In the liquid-suction heat exchanger cycle the additional subcooling produced by the heat exchanger caused the 35°C (95°F) expansion valve setting to be more restrictive than the unmodified cycle. Therefore, at the 27.8°C (82°F) test the indoor coil was starved even more with the liquid-suction heat exchanger.

Because of the performance penalty suffered by the liquid-suction heat exchanger cycle at the 27.8°C (82°F) test condition, the test procedure was modified by adjusting the expansion valve at the 27.8°C (82°F) test condition. This test is marked with an asterisk in Table 5. The valve was adjusted so that the vapor entering the liquid-suction heat exchanger was as close as possible to being saturated. The 35°C (95°F) test was then operated at the same valve setting. Table 7 shows that this method of expansion valve adjustment produces better performance at the 27.8°C (82 °F) test condition with a 35°C (95°F) performance virtually identical to the other valve adjustment method.

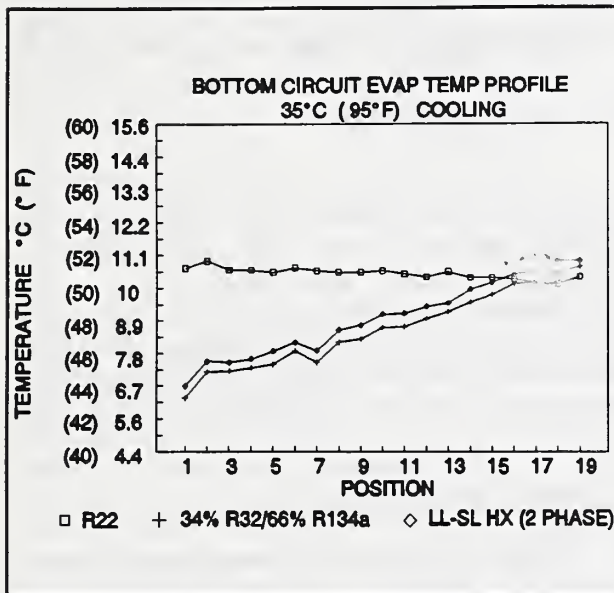
#### ANALYSIS OF SINGLE PHASE LIQUID-SUCTION HEAT EXCHANGE RESULTS

Table 7 shows that the performance increase for the single phase liquid-suction heat exchange cycle is two percent for both capacity and COP. However, it may be possible to increase this performance benefit by resizing the liquid-suction heat exchanger. Referring back to Figure 5, we recall that the enthalpy increments 1-1' and 3-3' must be equal. The absolute value of these enthalpy changes represents the amount of heat transferred in the liquid-suction heat exchanger. From basic heat exchanger theory, the amount of heat transferred is limited by the fluid stream with the smaller heat capacity. Where heat capacity is the product of mass flow and specific heat. Since the mass flows on both sides of the heat exchanger are equal, and since the liquid specific heat of the binary mixture is approximately 50% greater than the vapor, the vapor is the limiting side of the heat exchanger. It has been shown that the maximum benefit from the heat exchanger will occur if the liquid-suction heat exchanger has an effectiveness of 100%

[1]. This implies that the exiting temperature of the limiting vapor side be raised up to the temperature of the entering liquid. In practice this is difficult to achieve because of the large heat exchange area required and the possibility of an extremely high compressor discharge temperature. In this experiment, the liquid-suction heat exchanger effectiveness was 34% at the 35°C (95°F) test condition.

## ANALYSIS OF TWO PHASE LIQUID-SUCTION HEAT EXCHANGE RESULTS

As was shown previously (see Figure 8), allowing two phase low pressure refrigerant to enter the liquid-suction heat exchanger under the assumption of a constant evaporator pressure decreases the average evaporation temperature. However, test results showed that the average evaporation temperature actually increases. This occurs because the constant evaporator pressure assumption is incorrect for a system with a fixed area expansion device operating at a constant source temperature. In Figures 20 and 21, the



**Figure 20** Bottom circuit With and Without Two-Phase Liquid-Suction Heat Exchange

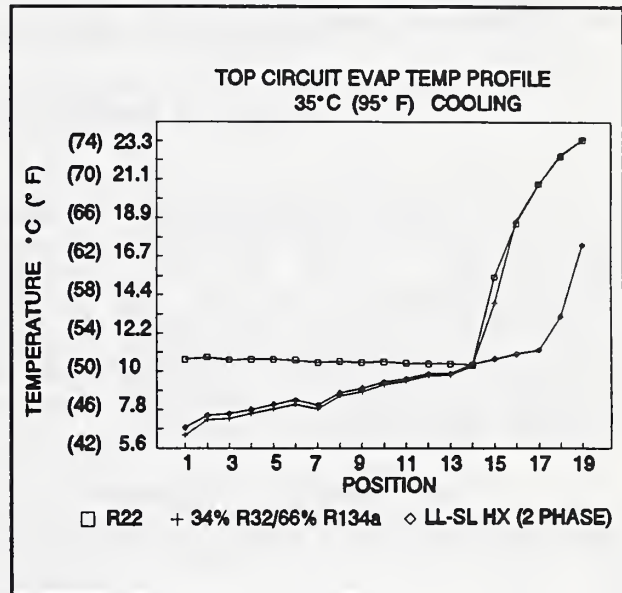


**Figure 21** Top Circuit With and Without Two-Phase Liquid-Suction Heat Exchange

evaporator temperature profiles are shown for R22 and the binary mixture without liquid-suction heat exchange and for the binary mixture with two phase liquid-suction heat exchange. The performance increase of the two-phase liquid suction heat exchange cycle for a fixed heat source temperature occurs because the evaporation pressure is increased. Since the high side pressure is fixed, the increased evaporator pressure causes a lower compression ratio and higher suction density. Both of these factors increase the system capacity and COP. The magnitude of the pressure increase and change in suction density are shown in Table 8.

**TABLE 8. EFFECT OF TWO PHASE LIQUID-SUCTION HEAT EXCHANGER**

	R22 NO HX	34% R32/66% R134a NO HX	34% R32/66% R134a TWO PHASE HX
$P_d$ kPa (psia)	1824 (264.5)	1927 (279.5)	1931 (280)
$P_s$ kPa (psia)	618 (89.7)	561 (81.3)	581 (84.3)
$\rho_s$ kg/m <sup>3</sup> (lb/ft <sup>3</sup> )	24.5339 (1.5316)	19.3295 (1.2067)	19.8789 (1.2410)

**TERNARY REFRIGERANT MIXTURE TEST**

An additional test was conducted with a ternary mixture of 30% R32, 10% R125 and 60% R134a by weight. Because of the performance improvement shown by the liquid-suction heat exchanger for the binary mixture, it was decided to test the ternary in a best performance mode with the liquid-suction heat exchanger. The ternary test results normalized by the R22 values are shown in Table 9. The performance of the ternary mixture is essentially the same as the binary mixture.

**TABLE 9. NORMALIZED TERNARY PERFORMANCE**

		NORMALIZED CAPACITY	NORMALIZED COP	NORMALIZED POWER
35°C (95°F)	HX 2- $\phi$	0.950	0.887	1.071

## GENERAL CONCLUSIONS REGARDING THE USE OF MIXTURES IN AIR-TO-AIR RESIDENTIAL HEAT PUMPS

Considerable work has been done to demonstrate the potential improvement in performance possible when a zeotropic mixture is used to match the temperature profile (glide) of the source and/or sink [8,9,10]. The improvement in system performance with glide matching occurs because of a reduction in the irreversibility associated with heat transfer through a finite temperature difference. A zeotropic mixture and counterflow heat exchangers are necessary to derive the maximum performance benefit from glide matching with a variable temperature source and sink. In a residential cooling only unit, it may be possible to design an indoor coil that approaches a pure counterflow arrangement. However, because of the way most residential condensing units are constructed it is likely that the outdoor coil will be in a nearly pure crossflow arrangement. What then are the theoretical performance implications of glide matching in a cooling only system configured so that the indoor coil (evaporator) is in pure counterflow and the outdoor coil (condenser) is in pure crossflow?

To gain a clear understanding of the concepts involved, the problem can be examined by using CYCLE11 with a simplified representation of the crossflow condenser. By considering the crossflow condenser to be an isothermal heat reservoir, the fundamental limits of a perfect glide match in one heat exchanger and a complete mismatch in the other can be examined. The isothermal reservoir model for the condenser is analogous to a condenser in any type of flow arrangement with a heat transfer fluid (HTF) of infinite heat capacity. The two limits of the simplified analysis are defined by a pure fluid and a zeotropic mixture with the same linear glide as the HTF of the counterflow evaporator. The pure refrigerant limit has a perfect glide match in the isothermal reservoir condenser and an extreme mismatch in the counterflow evaporator. The other limit is set by a zeotropic mixture that has a perfect glide match in the counterflow evaporator and an extreme mismatch in the isothermal reservoir condenser. The temperature glide of the evaporator HTF will be fixed by the application of residential cooling at 11.1°C (20°F) (from 26.7°C (80°F) to 15.6°C (60°F)).

At this point, a comment should be made regarding the ability of a refrigerant to match a 11.1°C (20°F) temperature glide in the counterflow evaporator. Since this is a significant glide, a binary refrigerant mixture would have to be composed of two pure components that are far apart in their normal boiling points. However, this also implies that the temperature glide will be highly nonlinear. Since CYCLE11 presumes that the temperature glide of the HTF is linear (a valid presumption since even air with condensation is approximately linear), glide matching with a highly non-linear refrigerant may be difficult for an air-to-air system.

The temperature glide of a binary mixture may be linearized by the addition of a third component whose normal boiling point is in between the other two. Therefore, the ternary mixture used in this CYCLE11 analysis was selected only on the basis of it having a linear temperature glide that matched the residential cooling application HTF glide of 11.1°C (20°F). The extent of the non-

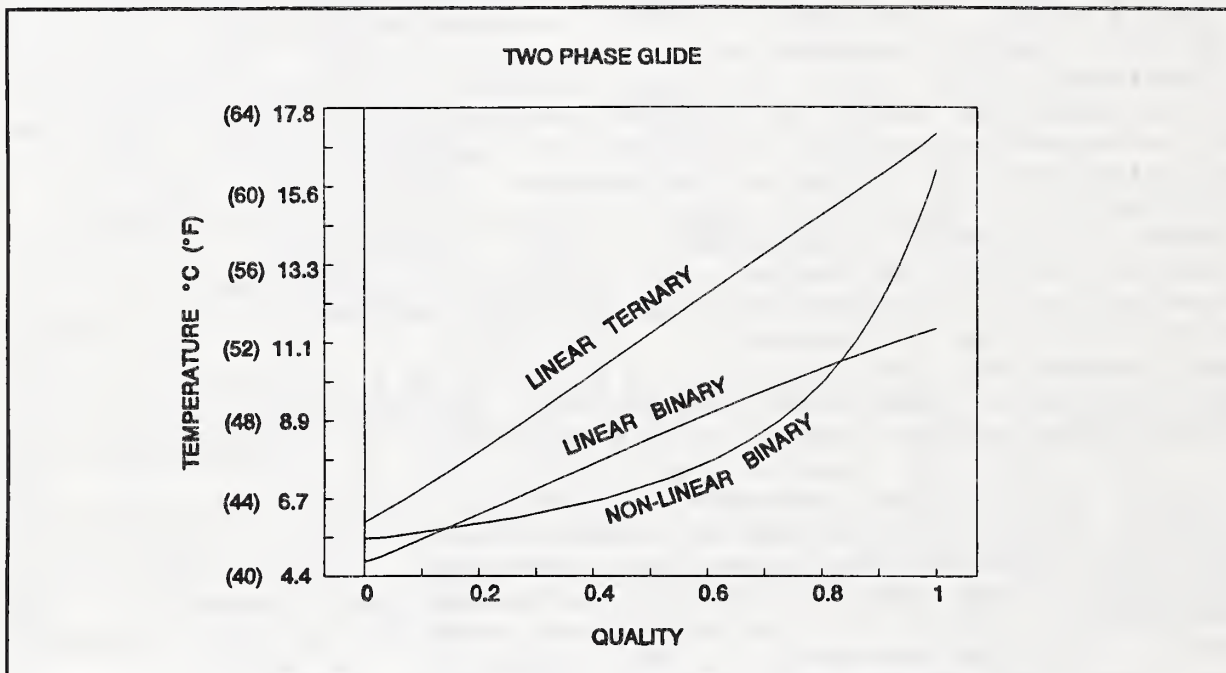


Figure 22 Linearization of Binary Mixture Glide by the Addition of a Third Component

linearity for a binary mixture with pure components far apart in normal boiling point and the ability of a third component to linearize the temperature glide is shown in Figure 22. The figure shows a binary mixture of 87% R22/13% R11 along with a linear ternary consisting of 45% R22/45% R142b/10% R11. An additional line for the mixture of 34% R32/66% R134a is shown to demonstrate that a binary mixture can be linear if the components normal boiling points are not too far apart.

To ensure that the comparisons were legitimate, all runs with the model were conducted to have the total UA per unit capacity ( $UA_t/Q_e$ ) equal to 0.2. This value is not meaningful in itself and was arbitrarily chosen to provide a basis for the comparisons. Although the criterion  $UA_t/Q_e=0.2$  provides a basis for comparing the two refrigerants, it is not enough to completely specify the terms of the comparison because it leaves unanswered the question of how the total UA should be distributed between the two heat exchangers. This extra degree of freedom is handled by plotting the results for COP versus the UA distribution. The UA distribution is defined as the fraction of the total UA (evaporator

plus condenser) in the evaporator ( $UA_e/UA_t$ ).

The results for the simplified condenser representation are shown in Figure 23 for pure R22 and a linear ternary of 45% R22/45% R142b/10% R11. The figure shows that glide matching in the counterflow evaporator with a linear mixture gives a higher COP than the pure fluid for  $UA_e/UA_t$  greater than 0.3. Additionally, the difference in COP between the linear mixture and the pure fluid

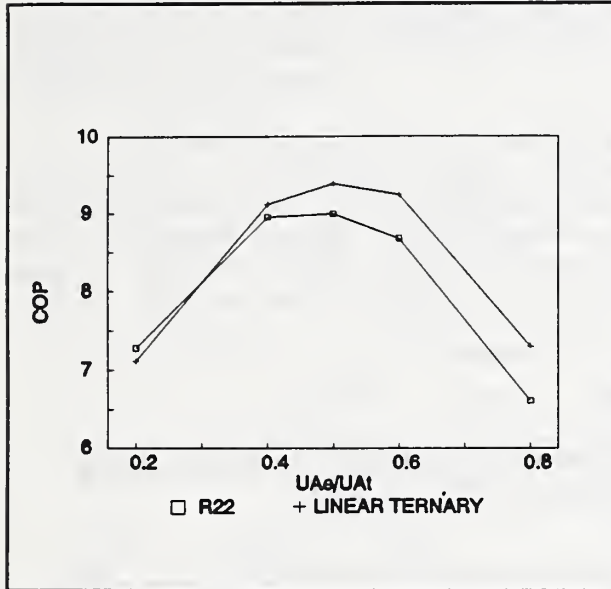


**Figure 23** Variation of COP With UA Distribution for the infinite Heat Capacity Condenser HTF Model

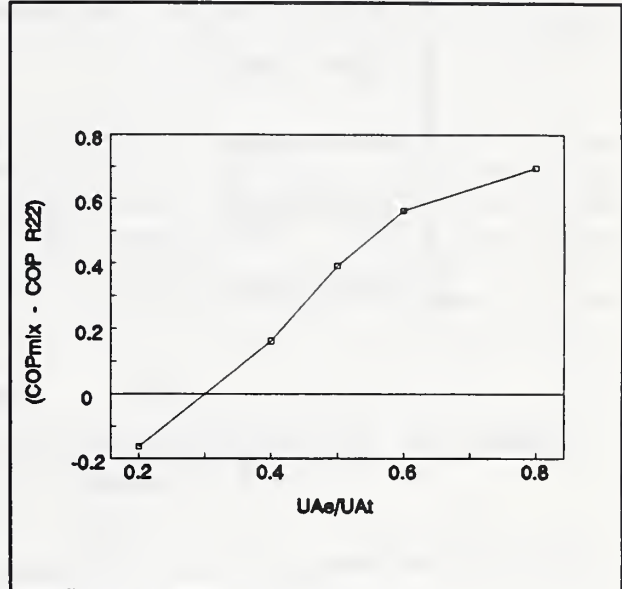


**Figure 24** COP Difference of the Two Glide Match Limits for the Infinite Heat Capacity Condenser HTF Model

increases as the ratio of  $UA_e/UA_t$  increases. This is shown in Figure 24 where the difference between the COP for the mixture and the COP for R22 is plotted against the UA distribution. Figure 23 also shows that the optimum UA distribution is very near to 0.5 despite the fact that the condenser heat duty is greater.

The variation of COP with UA distribution is determined by the cycle total irreversibility at each UA distribution. The total irreversibility can be quantified with respect to magnitude and origin by examining the entropy generated in each system component at each UA distribution. Since the compressor was modelled as isentropic and there are no pressure drops, the only sources of entropy generation are the expansion device, evaporator and condenser. The component and total entropy generation for R22 and the linear ternary of 45% R22/45% R142b/10% R11 is shown in Figures 25 and 26, respectively. The entropy generated by the expansion process is nearly identical in both figures. The heat exchanger entropy generation (evaporator and condenser) also exhibits the

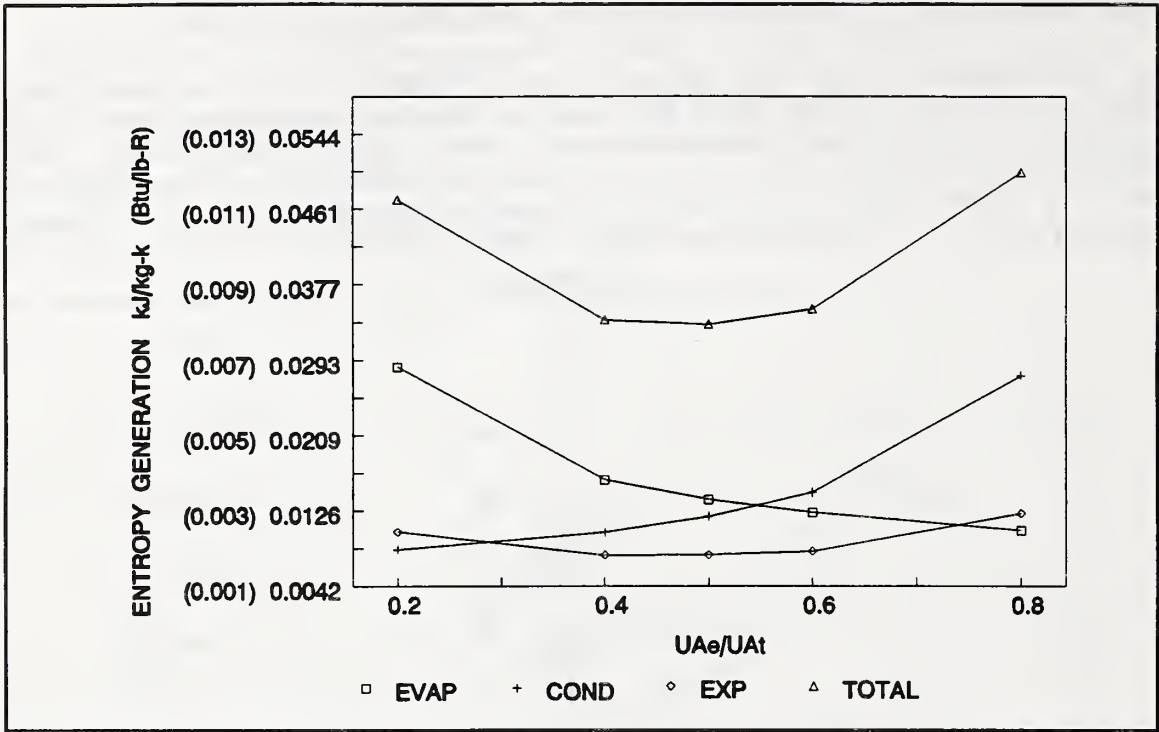


Figure 25 R22 Component Entropy Generation for the Infinite Heat Capacity Condenser HTF Model

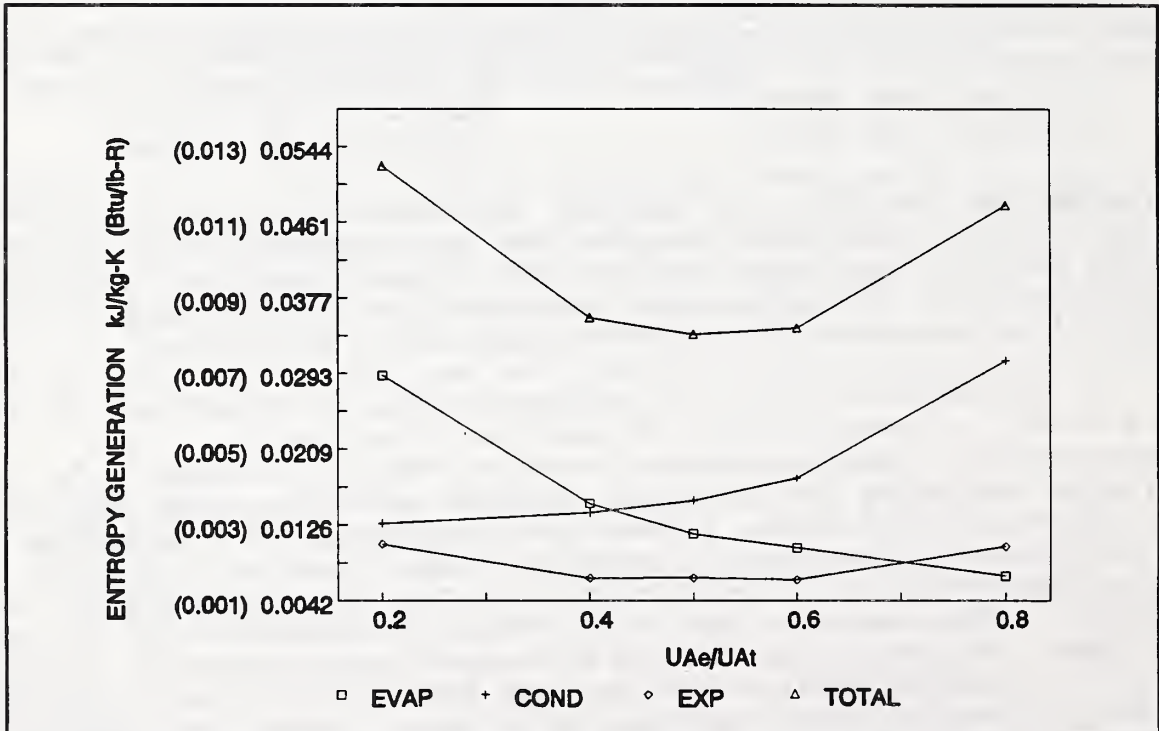


Figure 26 Linear Ternary Component Entropy Generation for the Infinite Heat Capacity Condenser HTF Model

same behavior with the variation in UA distribution in both figures. The two figures differ only at the extreme endpoints of the UA distribution. As expected, the entropy generation in the condenser is smallest when the condenser is large ( $UA_e/UA_t$  is small) and the isothermal phase change of the pure fluid matches the isothermal profile of the condenser HTF. Conversely, the entropy generated in the evaporator is the least when the evaporator is large ( $UA_e/UA_t$  is large) and the linear ternary glide matches the linear glide of the evaporator HTF. The increase in COP of the ternary mixture over pure R22 shown in Figure 23 occurs because the total entropy generated is lower for the mixture as  $UA_e/UA_t$  increases.

The second method of representing the crossflow condenser used a version of CYCLE11 which was modified to simulate crossflow or counterflow heat exchangers. In this case, the HTF glide for both the evaporator and condenser must be specified. The glides were again set by the application of residential cooling at 11.1°C (20°F) (from 26.7°C (80°F) to 15.6°C (60°F)) for the evaporator and

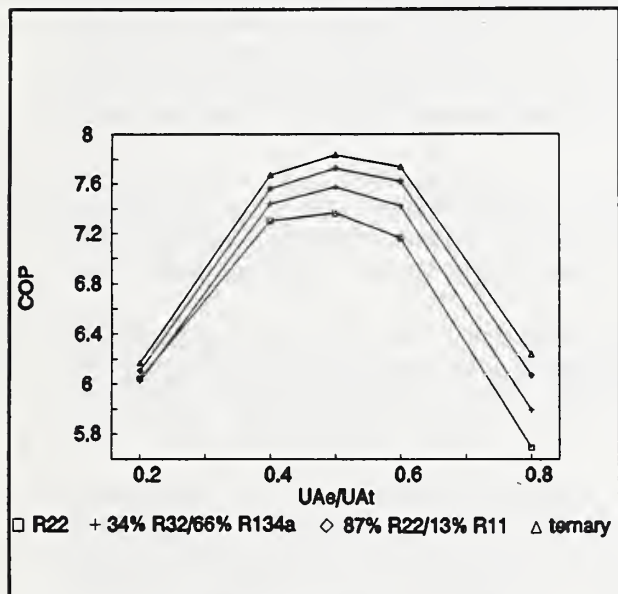


Figure 27 Variation of COP With UA Distribution for the Crossflow Condenser model

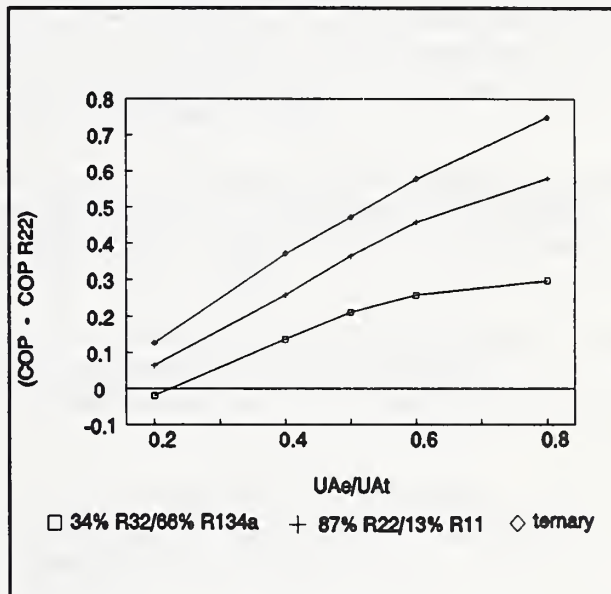


Figure 28 Difference in COP Between Each Mixture and R22 for Crossflow Condenser Model

8.3°C (15°F) (from 35°C (95°F) to 43.3°C (110°F)) for the condenser. The results for the CYCLE11 model of crossflow are presented in Figure 27 as a plot of COP versus UA distribution. Similar to Figure 24, the difference in COP between each fluid and R22 is shown in Figure 28. In addition to the limiting glide match fluids R22 and the linear ternary, the binary mixtures of 34% R32/66% R134a (5.6°C (10°F) glide) and 87% R22/13% R11 (11.1°C (20°F) nonlinear glide) are also shown in figures 27 and 28. As

expected the temperature glides of these fluids causes them to perform in between the two limiting cases. The component entropy generation plots for the realistic CYCLE11 crossflow representation are similar to those of the simplified condenser model and are not shown.

The preceding analysis shows that for an air-to-air unit with a counterflow evaporator and a crossflow condenser, with HTF temperature glides fixed by the application of residential cooling, the use of a zeotropic mixture to match glides in a counterflow evaporator is beneficial to performance. Converting the results of Figure 28 to a percentage basis shows that the COP of the linear ternary is 6.4% higher than R22 at  $UA_e/UA_t=0.5$ . The difference is even more pronounced as  $UA_e/UA_t$  increases. At  $UA_e/UA_t=0.8$  the linear ternary COP is 11.6% higher than R22.

## REFERENCES

1. Domanski, P.A., Didion, D.A., and Doyle, J.P., "Evaluation of Suction Line-Liquid Line Heat Exchange In the Refrigeration Cycle," Proceedings of the 1992 International Refrigeration Conference - Energy Efficiency and New Refrigerants, Purdue University, West Lafayette, Indiana, July 14-17, 1992.
2. Pannock, J., and Didion, D., "The Performance of Chlorine-Free Binary Zeotropic Refrigerant Mixtures in a Heat pump," NISTIR 4748, National Institute of Standards and Technology, Gaithersburg, Maryland, 1991.
3. Rothfleisch, P.I., and Didion, D.A., "A Performance Evaluation of a Variable Speed, Mixed Refrigerant Heat Pump," NISTIR 4597, National Institute of Standards and Technology, Gaithersburg, Maryland, 1991.
4. Vakil, H.B., "Thermodynamics of Heat Exchange in Refrigeration Cycles With Non-Azeotropic Mixtures - Part II: Suctionline Heat Exchange and Evaporative Cooling of Capillary," Proceedings of the XVI International Congress of Refrigeration, International Institute of Refrigeration, Paris, France, 1983.
5. Aaron, D., and Domanski, P., "An Experimental Investigation and Modeling of the Flow Rate of Refrigerant 22 Through the Short Tube Restrictor," NISTIR 4120, National Institute of Standards and Technology, Gaithersburg, Maryland, 1989.
6. McLinden, M.O., and Radermacher, R. "Methods for Comparing the Performance of Pure and Mixed Refrigerants In the Vapor Compression Cycle," International Journal of Refrigeration, Vol. 10, November 1987.
7. Domanski, P.A., and McLinden, M.O., "A Simplified Cycle Simulation Model for the Performance Rating of Refrigerants and Refrigerant Mixtures," International Journal of Refrigeration, Vol. 15, No. 2, 1992.
8. Didion, D.A., and Bivens, D.B., "The Role of Refrigerant Mixtures as Alternatives," Proceedings of the ASHRAE CFC Technology Conference, National Institute of Standards and Technology, Gaithersburg, Maryland, 1989.
9. Chwalowski, M., "Evaporator Performance Investigation for Residential Air-Conditioning Application Using Mixed Refrigerants," NISTIR 4723, National Institute of Standards and Technology, Gaithersburg, Maryland, 1991.

10. Mulroy, W., and Didion, D.A., "The Performance of A Conventional Residential Sized Heat Pump Operating With A Nonazeotropic Binary Refrigerant Mixture," NBSIR 86-3422, National Institute of Standards and Technology, Gaithersburg, Maryland, 1986.

## APPENDIX A

### UNCERTAINTY ANALYSIS OF STEADY STATE HEATING TEST

If we consider the result  $R$  to be a function of  $n$  independent variables  $V_1, V_2, \dots, V_n$  and each of the independently measured variables has an uncertainty  $\Delta V_1, \Delta V_2, \dots, \Delta V_n$ , then the uncertainty in the result  $\Delta R$  is given by:

$$\Delta R = \left[ \left( \frac{\partial R}{\partial V_1} \Delta V_1 \right)^2 + \left( \frac{\partial R}{\partial V_2} \Delta V_2 \right)^2 + \dots + \left( \frac{\partial R}{\partial V_n} \Delta V_n \right)^2 \right]^{1/2} \quad (1)$$

This equation can be nondimensionalized to express the uncertainty on a percentage basis by dividing through by  $R$ .

$$\frac{\Delta R}{R} = \left[ \left( \frac{\partial R}{\partial V_1} \frac{\Delta V_1}{R} \right)^2 + \left( \frac{\partial R}{\partial V_2} \frac{\Delta V_2}{R} \right)^2 + \dots + \left( \frac{\partial R}{\partial V_n} \frac{\Delta V_n}{R} \right)^2 \right]^{1/2} \quad (2)$$

When written in a form analogous to ASHRAE Standard 116-1983, the equation for the steady state heating capacity  $Q_H$  (kW) is:

$$Q_H = \sqrt{2} \cdot C \cdot A (Cp_a + Cp_w \cdot W_n) (T_2 - T_1) \left[ \frac{P_s P_n}{RT_n (1 + W_n)} \right]^{1/2} \quad (3)$$

where:

- $C$  = nozzle discharge coefficient - 0.99
- $A$  = nozzle throat area -  $m^2$
- $W_n$  = nozzle humidity ratio -  $kg\ H_2O/kg\ da$
- $T_2 - T_1$  = indoor coil air temperature rise -  $^{\circ}C$
- $P_s$  = static pressure drop across nozzle - Pa
- $P_n$  = nozzle throat absolute barometric pressure - Pa
- $R$  = ideal gas constant for air -  $286.987\ J/kg-K$
- $T_n$  = nozzle throat air temperature - K
- $Cp_a$  = specific heat of air -  $1.005\ kJ/kg_{da}-^{\circ}C$  @ 300K
- $Cp_w$  = specific heat of water -  $1.8629\ kJ/kg_w-^{\circ}C$  @ 300K

Calculate the required partial derivatives:

$$\frac{\partial Q_H / \partial A}{Q_H} = \frac{1}{A}$$

$$\frac{\partial Q_H / \partial W_n}{Q_H} = \frac{\frac{Cp_w}{2} W_n + Cp_w - \frac{Cp_a}{2}}{Cp_w W_n^2 + (Cp_w + Cp_a) W_n + Cp_a}$$

$$\frac{\partial Q_H / \partial (T_2 - T_1)}{Q_H} = \frac{1}{T_2 - T_1}$$

$$\frac{\partial Q_H / \partial P_s}{Q_H} = \frac{1}{2P_s}$$

$$\frac{\partial Q_H / \partial P_n}{Q_H} = \frac{1}{2P_n}$$

$$\frac{\partial Q_H / \partial T_n}{Q_H} = \frac{-1}{2 T_n}$$

Rewriting Equation (2) for  $\Delta Q_H / Q_H$  gives:

$$\begin{aligned} \frac{\Delta Q_H}{Q_H} = & \left[ \left( \frac{\partial Q_H / \partial A}{Q_H} \Delta A \right)^2 + \left( \frac{\partial Q_H / \partial W}{Q_H} \Delta W_n \right)^2 \right. \\ & + \left. \left( \frac{\partial Q_H / \partial (T_2 - T_1)}{Q_H} \Delta (T_2 - T_1) \right)^2 + \left( \frac{\partial Q_H / \partial P_s}{Q_H} \Delta P_s \right)^2 \right. \\ & \left. + \left( \frac{\partial Q_H / \partial P_n}{Q_H} \Delta P_n \right)^2 + \left( \frac{\partial Q_H / \partial T_n}{Q_H} \Delta T_n \right)^2 \right]^{1/2} \end{aligned} \quad (4)$$

Equation (4) can be evaluated to give the uncertainty in  $Q_H$  as a percentage of the experimental value for  $Q_H$  provided that each of the individual uncertainties are known. Since  $A_n$ ,  $(T_2 - T_1)$ ,  $P_s$ ,  $P_n$  and  $T_n$  are all directly measured quantities their respective uncertainties are known. However,  $W_n$  is a calculated result so the uncertainty in  $W_n$  must first be calculated from Equation (1).

The expression for the humidity ratio  $W_n$  is

$$W_n = 0.62198 \frac{P_w}{P - P_w}$$

where:

$P$  = absolute barometric pressure - Pa  
 $P_w$  = saturation pressure of water at the dewpoint temperature - Pa

$P$  is a directly measured result but  $P_w$  is another calculated result. The expression for  $P_w$  (valid from 0°C to 200°C) is

$$P_w = \text{EXP} \left[ \frac{C_8}{T_d} + C_9 + C_{10} T_d + C_{11} T_d^2 + C_{12} T_d^3 + C_{13} \ln (T_d) \right]$$

where:

$$\begin{aligned} T_d &= \text{dew point temperature} - \text{K} \\ C_8 &= -5.800\ 220\ 6\ \text{E}\ 3 \\ C_9 &= 1.391\ 499\ 3 \\ C_{10} &= -4.864\ 023\ 9\ \text{E}\ -\ 2 \\ C_{11} &= 4.176\ 476\ 8\ \text{E}\ -\ 5 \\ C_{12} &= -1.445\ 209\ 3\ \text{E}\ -\ 8 \\ C_{13} &= 6.545\ 967\ 3 \end{aligned}$$

Therefore, the uncertainty in  $P_w$  can be evaluated from Equation (1). The required partial derivative is:

$$\frac{\partial P_w}{\partial T_d} = \left[ \frac{-C_8}{T_d^2} + C_{10} + C_{11} T_d + 3C_{12} T_d^2 + \frac{C_{13}}{T_d} \right] P_w$$

Therefore, the uncertainty in  $P_w$  ( $\Delta P_w$ ) is given by

$$\Delta P_w = \left[ \left( \frac{\partial P_w}{\partial T_d} \Delta T_d \right)^2 \right]^{1/2} = \frac{\partial P_w}{\partial T_d} \Delta T_d \quad (5)$$

the necessary measured values and uncertainties from the 8.33°C (47°F) R22 heating test are

$$\begin{aligned} P_w &= 1382.4\ \text{Pa} \\ T_d &= 284.93\ \text{K} \\ \Delta T_d &= \pm 0.15^\circ\text{C} \quad (\text{manufacturer specified uncertainty}) \end{aligned}$$

evaluating Equation (5) yields

$$\Delta P_w = \pm 11.23026\ \text{Pa}$$

The uncertainty in  $W_n$  can now be evaluated. From the expression for  $W_n$  the required partial derivatives are

$$\frac{\partial W_n}{\partial P} = 0.62198 \frac{P_w}{(P - P_w)^2}$$

$$\frac{\partial W_n}{\partial P_w} = 0.62198 \frac{P}{(P - P_w)^2}$$

therefore, the uncertainty in  $W_n$  is given by

$$\Delta W_n = \left[ \left( \frac{\partial W_n}{\partial P} \Delta P \right)^2 + \left( \frac{\partial W_n}{\partial P_w} \Delta P_w \right)^2 \right]^{1/2} \quad (6)$$

the necessary measured values and uncertainties from the 8.33°C (47 °F) heating test are

$$\begin{aligned} P &= 99661.9 \text{ Pa} \\ P_w &= 1382.4 \text{ Pa} \\ \Delta P &= \pm 45.72 \text{ Pa} \quad (\text{manufacturer specified uncertainty}) \\ \Delta P_w &= \pm 11.23026 \text{ Pa} \quad (\text{calculated result}) \end{aligned}$$

Evaluating Equation (6) yields

$$\Delta W_n = \pm 7.21873 \text{ E-5 kg H}_2\text{O/kg}_{\text{da}}$$

Using the data from the 8.33°C (47°F) R22 heating test, Equation (4) can now be evaluated. The necessary measured values are:

$$\begin{aligned} A &= 0.012871 \text{ m}^2 \\ W_n &= 0.008749 \text{ kg H}_2\text{O/kg}_{\text{da}} \\ T_2 - T_1 &= 15.94 \text{ }^\circ\text{C} \quad (\text{measured by thermopile}) \\ P_g &= 75.678 \text{ Pa} \\ P_n &= 99586.2 \text{ Pa} \\ T_n &= 310.1 \text{ K} \end{aligned}$$

The uncertainties are:

$$\begin{aligned} \Delta A &= \pm 5.0 \text{ E-5 m}^2 \quad (\text{k=3 std. deviations of the mean}) \\ \Delta W_n &= \pm 7.21873 \text{ E-5 kg H}_2\text{O/kg}_{\text{da}} \quad (\text{calculated result}) \\ \Delta(T_2 - T_1) &= \pm 0.28 \text{ }^\circ\text{C} \quad (\text{complies with ANSI/ASHRAE Std. 41.1-1986}) \\ \Delta P_g &= \pm 2.48 \text{ Pa} \quad (\text{manufacturer specified uncertainty}) \\ \Delta P_n &= \pm 45.72 \text{ Pa} \quad (\text{manufacturer specified uncertainty}) \\ \Delta T_n &= \pm 0.28 \text{ K} \quad (\text{complies with ANSI/ASHRAE Std. 41.1-1986}) \end{aligned}$$

The uncertainty of a temperature difference would normally be greater than that of a single measurement. For thermocouples, the uncertainty of the difference is larger because there are two voltage measurements required. If a thermopile is used instead, then only one voltage measurement is required. Therefore, the error of a thermopile is equal to a single absolute temperature measurement. Evaluating the partial derivatives and substituting into Equation (4) yields:

$$\frac{\Delta Q_H}{Q_H} = 0.024 = 2.4\%$$

## APPENDIX B

### UNCERTAINTY ANALYSIS OF STEADY STATE COOLING TEST

The equation for steady state cooling capacity,  $Q_C$  (kW) is:

$$Q_C = Q_S + Q_L \quad (7)$$

where:

$Q_S$  = sensible cooling capacity (kW)

$Q_L$  = latent cooling capacity (kW)

The uncertainty in  $Q_C$  is given by eq. (1) as:

$$\Delta Q_C = \left[ \left( \frac{\partial Q_C}{\partial Q_S} \Delta Q_S \right)^2 + \left( \frac{\partial Q_C}{\partial Q_L} \Delta Q_L \right)^2 \right]^{1/2} \quad (8)$$

$$\text{since } \partial Q_C / \partial Q_S = \partial Q_C / \partial Q_L = 1$$

$$\Delta Q_C = [ (\Delta Q_S)^2 + (\Delta Q_L)^2 ]^{1/2} \quad (9)$$

When written in a form analogous to ASHRAE Standard 116-1983,  $Q_S$  and  $Q_L$  are given by:

$$Q_S = \sqrt{2} \cdot C \cdot A [Cp_a + Cp_w W] (T_2 - T_1) \left[ \frac{P_s P_n}{R T_n (1 + W_n)} \right]^{1/2} \quad (10)$$

This equation is the same as the steady state heating capacity given by Equation (3). Therefore, the uncertainty in  $Q_S$  is given by Equation (4).

$$\frac{\Delta Q_S}{Q_S} = \frac{\Delta Q_H}{Q_H} = 0.024 \quad (11)$$

$$Q_L = \sqrt{2} \cdot C \cdot A \cdot h_{fg} \left[ \frac{P_s P_n}{R T_n (1 + W_n)} \right]^{1/2} (W_r - W_n) \quad (12)$$

where:

$W_r$  = room humidity ratio

$W_n$  = nozzle humidity ratio

$h_{fg}$  = latent heat of water - 2465.9 kJ/kg @ 15°C

The required partial derivatives are:

$$\frac{\partial Q_L}{\partial A} = \sqrt{2} \cdot C \cdot h_{fg} \left[ \frac{P_s P_n}{R T_n (1 + W_n)} \right]^{1/2} (W_r - W_n)$$

$$\frac{\partial Q_L}{\partial P_s} = \frac{\sqrt{2}}{2} \cdot C \cdot A \cdot h_{fg} \left[ \frac{P_n}{P_s R T_n (1 + W_n)} \right]^{1/2} [W_r - W_n]$$

$$\frac{\partial Q_L}{\partial P_n} = \frac{\sqrt{2}}{2} \cdot C \cdot A \cdot h_{fg} \left[ \frac{P_s}{P_n R T_n (1 + W_n)} \right]^{1/2} [W_r - W_n]$$

$$\frac{\partial Q_L}{\partial T_n} = \frac{-\sqrt{2} \cdot C \cdot A \cdot h_{fg}}{2 T_n^{3/2}} \left[ \frac{P_s P_n}{R (1 + W_n)} \right]^{1/2} [W_r - W_n]$$

$$\frac{\partial Q_L}{\partial W_r} = \sqrt{2} \cdot C \cdot A \cdot h_{fg} \left[ \frac{P_s P_n}{R T_n (1 + W_n)} \right]^{1/2}$$

$$\frac{\partial Q_L}{\partial W_n} = \frac{-\sqrt{2}}{2} \cdot C \cdot A \cdot h_{fg} \left[ \frac{P_s P_n}{R T_n} \right]^{1/2} \left[ \frac{2 + W_r + W_n}{(1 + W_n)^{3/2}} \right]$$

Rewriting Equation (1) for  $\Delta Q_L$  gives

$$\Delta Q_L = \left[ \left( \frac{\partial Q_L}{\partial A} \Delta A \right)^2 + \left( \frac{\partial Q_L}{\partial P_s} \Delta P_s \right)^2 + \left( \frac{\partial Q_L}{\partial P_n} \Delta P_n \right)^2 + \left( \frac{\partial Q_L}{\partial T_n} \Delta T_n \right)^2 + \left( \frac{\partial Q_L}{\partial W_r} \Delta W_r \right)^2 + \left( \frac{\partial Q_L}{\partial W_n} \Delta W_n \right)^2 \right]^{1/2} \quad (13)$$

The necessary measured values from the 35 °C (95 °F) cooling test are:

$$\begin{aligned} A &= 0.012871 \text{ m}^2 \\ P_s &= 74.365 \text{ Pa} \\ P_n &= 100068.9 \text{ Pa} \\ T_n &= 288.9 \text{ K} \\ W_r &= 0.011362 \text{ kg H}_2\text{O/kg da} \\ W_n &= 0.009826 \text{ kg H}_2\text{O/kg da} \\ Q_s &= 1.918 \text{ kW} \\ Q_L &= 0.637 \text{ kW} \end{aligned}$$

The estimated uncertainties are (see appendix A for source):

$$\begin{aligned}\Delta A &= \pm 5.0 \text{ E-5 } \text{ m}^2 \\ \Delta P_s &= \pm 2.48 \text{ Pa} \\ \Delta P_n &= \pm 45.72 \text{ Pa} \\ \Delta T_n &= \pm 0.28 \text{ K} \\ \Delta W_n = \Delta W_R &= \pm 7.21873 \text{ E-5 } \text{ kg H}_2\text{O/kg da}\end{aligned}$$

Evaluating the partial derivatives and substituting into Equation (13) yields:

$$\Delta Q_L = 0.0442 \text{ kW}$$

Expressing the uncertainty as a percentage of  $Q_L$  gives

$$\frac{\Delta Q_L}{Q_L} = \frac{0.0442}{0.637} = 0.0694 = 6.94\%$$

From Equation (11)

$$\Delta Q_S = 0.024 (1.918 \text{ kW}) = 0.046 \text{ kW}$$

From Equation (9)

$$\Delta Q_C = [(0.046)^2 + (0.0442)^2]^{1/2} = 0.0638 \text{ kW}$$

Expressing the uncertainty as a percentage of  $Q_C$  gives

$$\frac{\Delta Q_C}{Q_C} = \frac{0.0638}{1.918 + 0.637} = 0.025 = 2.5\%$$





